LA-UR-12-00121

Title: Testing for the Photon Doppler Broadening Data Sampling Bug in MCNP5/X

Author(s):
Brian C. Kiedrowski
Forrest B. Brown
Morgan C. White
D. Kent Parsons

Intended for: MCNP Documentation

Testing for the Photon Doppler Broadening Data Sampling Bug in MCNP5/X

Brian C. Kiedrowski, Forrest B. Brown,
Morgan C. White, D. Kent Parsons

1 Introduction

MCNP5/X has the capability to perform photon Doppler broadening to incorporate the effect of bound electrons on photon scattering. This effect is generally important if energy spectra or detector responses are desired for photons in the tens to hundreds of keV energy range. In the Fall of 2011, a diligent MCNP user noticed that the sampling routines in MCNP were inconsistent with the data for sampling which atomic shell the electron is bound. The data are provided in probability density function (PDF) format, whereas MCNP sampled the data as if they are in a cumulative density function (CDF) format, leading to erroneous results.

Future versions of MCNP (i.e., MCNP6) will internally convert the PDF data into CDF data and the sampling will be performed consistently. However, to support existing users so that they do not have to update and revalidate a new version of MCNP, new data files have been provided with the atomic shells in CDF representation, which will allow versions prior to MCNP6 to account for photon Doppler broadening correctly. The details of the new data libraries are discussed in Los Alamos memo LA-UR-12-00018, "Further Notes on MCPLIB03/04 and New MCPLIB63/84 Compton Broadening Data For All Versions of MCNP5". For the purposes of this report, the old data have the extensions of .03p and .04p, whereas the new temporary data have the corresponding extensions .63p and .84p.

Before releasing the new data files, testing has been performed to both assess the quality of the new data and the impact of the fix to inform users if they need to upgrade their data libraries. Hundreds of CPU hours of testing was performed by the MCNP development team in addition to that done by the LANL data team, and the general conclusion is that the effect on the spectra is generally small, but noticeable. Furthermore, as a general trend, the previous, incorrect method in MCNP was doing too little Doppler broadening. The new data will generally produce results with even smoother edges than previously predicted.

Note that this does not necessarily mean the answers are more predictive of reality, it merely means that MCNP is correctly sampling the data as provided. It may be in some cases the new data might produce worse answers because the atomic shell probability sampling is done strictly on the number of electrons occupying each atomic shell and does not account for any screening effects. In either case, users that care about detailed photon detector spectra in the tens to hundreds of keV energy range are encouraged to update.

2 Description of the Tests

Six types of tests are performed to assess the quality of the data. The test problems are run with only .04p and .84p sets unless otherwise noted. The tests are as follows:

1) The first set of tests assesses what values the incorrect sampling of the data is returning within MCNP. The PDF and CDF data is randomly sampled as MCNP does numerous times and the frequency of sampling each shell is obtained.

2) Short 100k history runs of all elements from Z = 1-100 to ensure that MCNP runs to completion and no serious errors are encountered. Both the .63p and .84p libraries are run.

3) For 30 selected elements (to span much of the periodic table, capture trends, and focus on common detector materials), a 90 keV photon source is placed in a 1 cm radius ball of matter at a density of 1.0 g/cc. These are run in MCNP for 1 billion histories each. The energy spectrum of the photon flux in the ball (F4 tally) and the photon energy deposition in the ball (F8 tally) are tallied. The thick-target bremsstrahlung approximation is used. The elements used are H, He, Li, Be, B, C, N, O, F, Na, Si, P, S, K, Ga, Ge, As, Br, Cd, In, Te, I, Cs, La, Ce, Nd, Lu, Hg, Pb, and U.

4) For 10 selected elements, a 195 keV photon beam is directed at a thin (nearly infinite in the z-direction with a thickness of 0.01 cm and density 1.0 g/cc) slab target using 100 million histories. The energy spectrum

of the backscattered photon current (F1 tally) is tallied. This simulation uses explicit electron transport modeling. The elements used are H, C, Na, Si, Fe, Ge, I, La, W, and U.

5) The photon energy flux spectrum and energy deposition for a 88 keV photon source on a SiLi detector using 1 billion histories. Explicit electron transport is performed.

6) The photon energy flux spectrum and energy deposition for a 80 keV photon source on a Ge detector using 100 million histories. Explicit electron transport is performed.

3 Results of the Tests

The results of the six test case types are given. The version of the software is MCNP5-1.60 with a threaded (OMP) and non-MPI compilation that is a direct copy of the DVD image distributed by RSICC. All the problems are run on a Linux AMD x84, 64-bit processor using four threads. The results are usually labeled "No Doppler .84p", "Doppler .04p", or "Doppler .84p". This means the new data with no Doppler broadening, the old data with the PDF representation, and the new temporary data with the CDF representation.

For brevity, this section gives plots of only a few of the results. Interested readers should consult Appendix A for a complete listing of figures.

1) The tests involving which shell is sampled by the bad sampling (of the PDF data, assuming the data are in CDF format) versus what is sampled with appropriate data shows a consistent trend of strongly oversampling the outermost shell. The oversampling tends to worsen as the atomic number Z increases. Tests show that the sampling on the new (CDF) data returns approximately (within statistical noise) of the actual sampling probabilities given by the PDF. Results iodine are shown in Fig. 1.a. The true probabilities (and what is sampled with CDF data) is given by the blue boxes and the bad sampling with the PDF data is given by the red lines. For iodine, many of the shells are not sampled at all currently, and about 90 percent of the time, the outermost shell is sampled, as opposed to the true sampling frequency of about 6 percent. Fig. 1.b shows the probability of sampling the outermost shell the correct and wrong methods. The general trend is that as Z increases, the discrepancy between what MCNP should have been sampling and what it did sample grows.

2) The tests of short 100k history runs of the new data from elements Z = 1-100 show that all run to completion with no errors. This is important for quality assurance purposes.

3) The results of the tests show a general trend that as Z increases, sampling the PDF as it was a CDF did not result in enough Doppler broadening. As a test on the data and sampling, hydrogen and helium are particularly interesting because there should be no impact from the fix since there is only one shell to sample. Indeed, both the old and the new data produce exactly the same result.

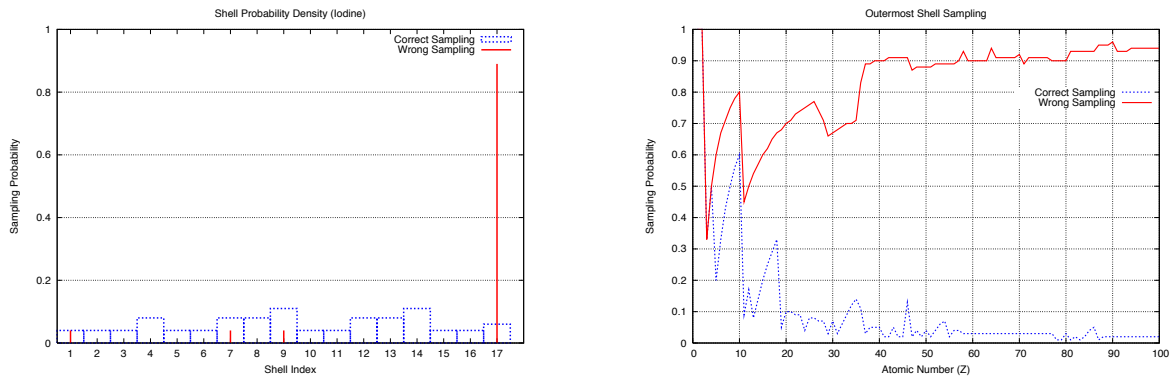

(a) (b)

Figure 1: (a) Sampling of shells for iodine. (b) Outermost shell sampling probabilities.

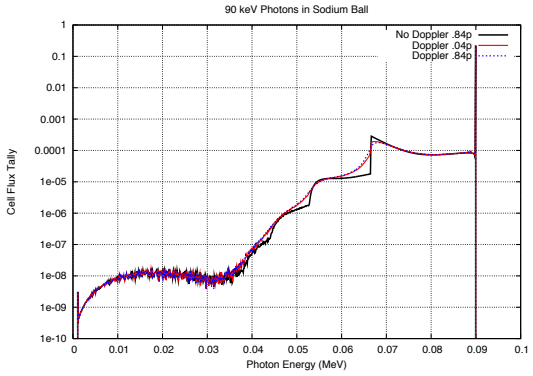

(a)

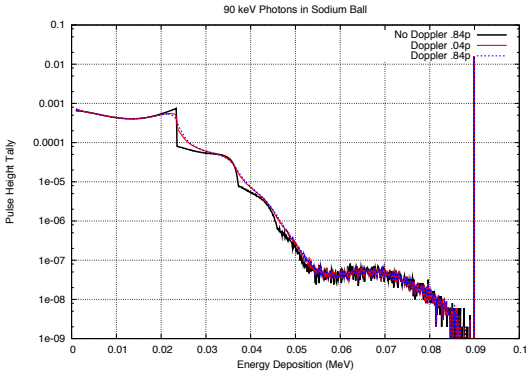

(b)

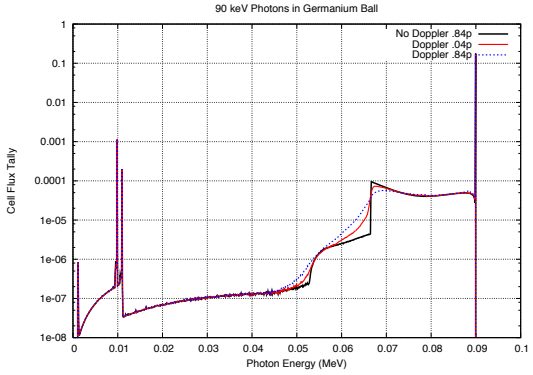

(c)

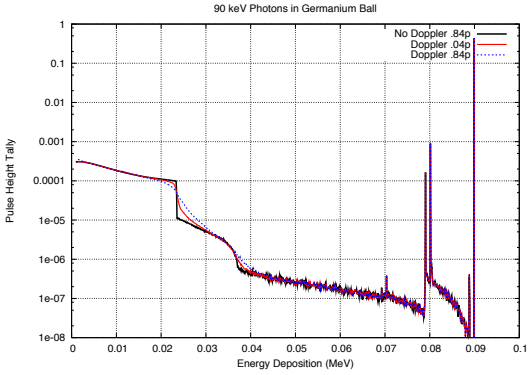

(d)

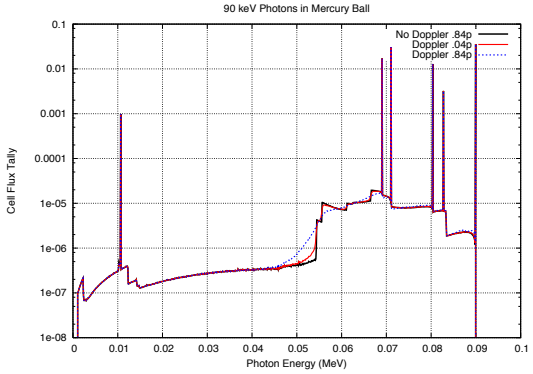

(e)

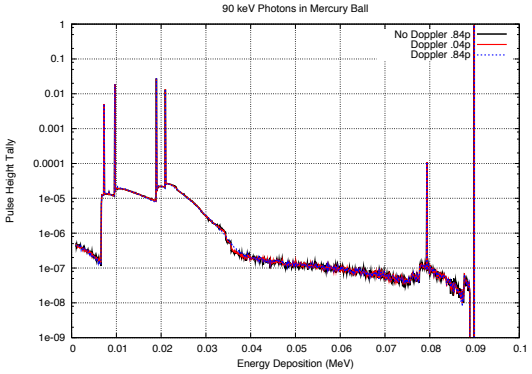

(f)

Figure 2: Cell flux and energy deposition tallies in balls of a few elements.

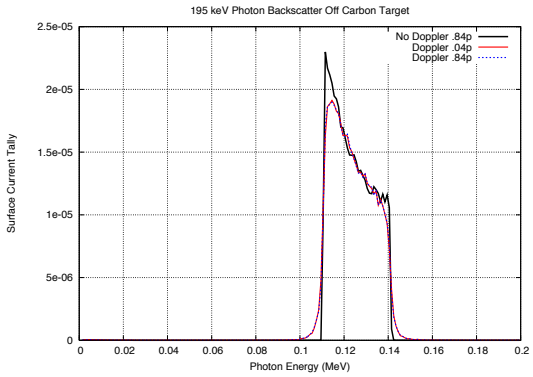

(a)

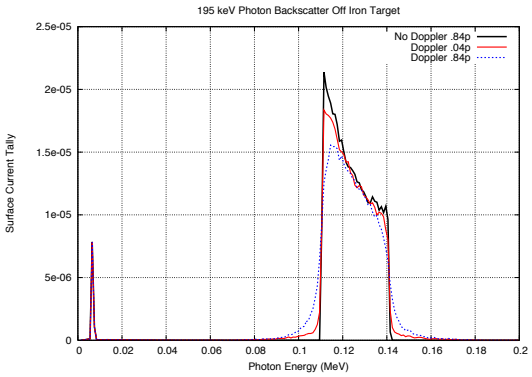

(b)

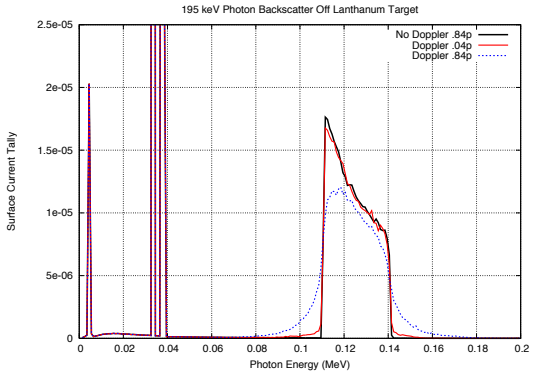

(c)

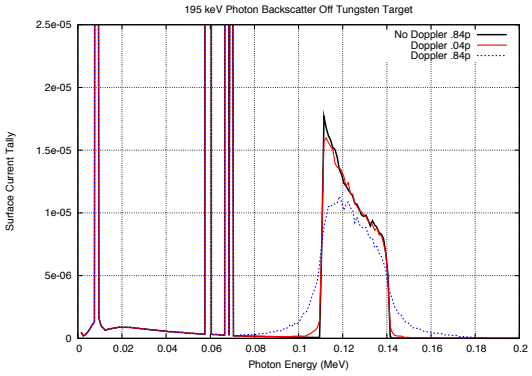

(d)

Figure 3: Photon backscatter off thin targets of a few elements.

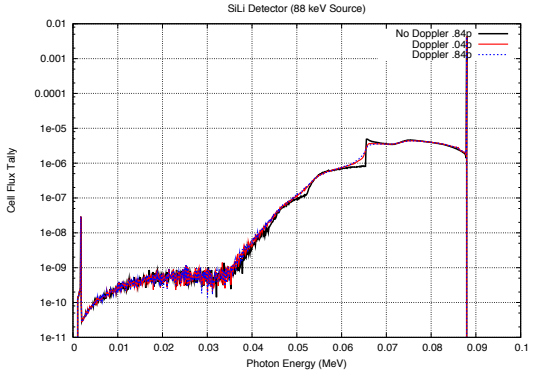

(a)

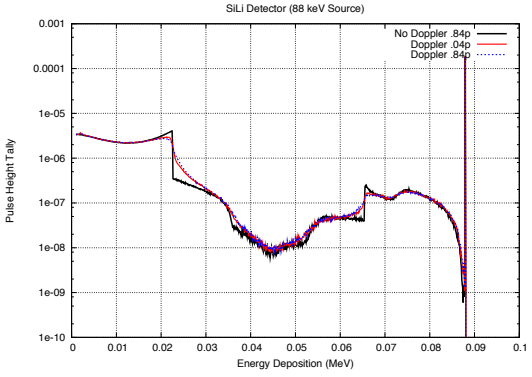

(b)

Figure 4: (a) Photon cell flux and (b) energy deposition inside SiLi detector.

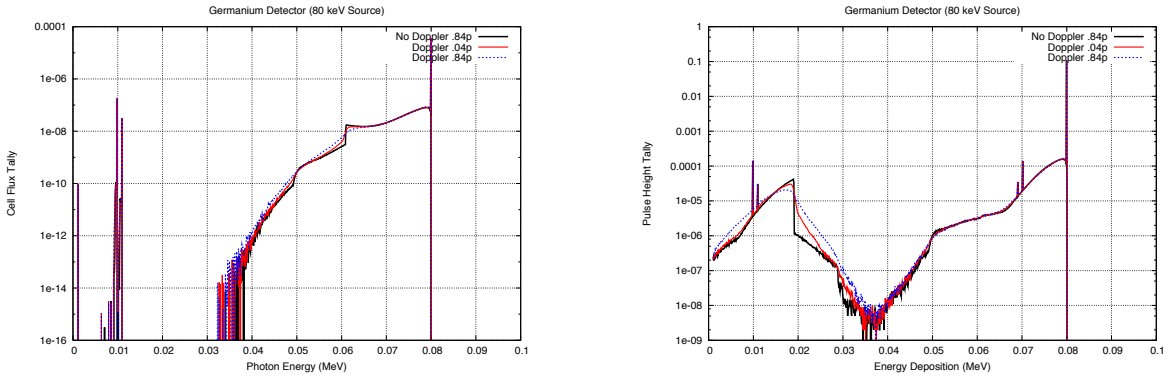

(a) (b)

Figure 5: (a) Photon cell flux and (b) energy deposition inside Ge detector.

Results of photon flux and energy deposition for sodium, germanium, and mercury are displayed in Fig. 2. For the flux tally, there is an increase in the amount of broadening observed in the Compton edges with increasing Z. For the energy deposition (analogous to a detector signal), it appears that germanium exhibits the most impact, and results of elements with similar Z such as gallium and arsenic show similar behavior. This is probably because of the intensity of the photopeak and other features versus the edges. For detector response type problems, materials such as gallium-arsenide and germanium are likely candidates for being prone to having different results.

4) The photon backscatter problems show a similar trend, that the gap between the amount of Doppler broadening MCNP should have been predicting to what it does with the CDF data increases with increasing Z. Results for carbon, iron, lanthanum, and tungsten are given in Fig. 3.

5) The photon flux and the photon plus electron energy deposition tallies for the SiLi detector are given in Fig. 4. It appears the differences are quite small around the edges, with a difference of less than ten percent. For most applications, this is probably a negligible difference. This confirms much of the observations seen in test groups 3 and 4; the differences there for the lighter elements are small for them as well.

6) The photon flux and the photon plus electron energy deposition tallies for the Ge detector are given in Fig. 5. The difference around the edge of the photon flux is about as large as 30 percent, which is typically quite small for this application. The difference around the lower energy edge of the energy deposition is about as large as 150 percent, which may by a large enough difference for a user to be concerned about.

4 Conclusion and Recommendation to Users

Versions prior to MCNP6 have a bug in the photon Doppler broadening routines that assumes CDF data, when they are in fact PDF data. Modified data sets with a .63p and .84p extensions have been released to provide a backward compatible fix to the issue. Several test problems have shown that the effect is that MCNP would overly select the outermost shell, and the issue becomes more extreme as Z increases. The effect on calculational results is that MCNP was doing less Doppler broadening than it should have been doing, and the effect tends to grow with increasing Z as well, but that depends on the problem.

Generally speaking, anyone concerned with photon detector spectra where the photons are in the energy ranges of tens to hundreds of keV should upgrade to the latest mcplib. Those interested only in neutron physics problems, or higher energy photons for shielding and dose applications are probably not impacted by this defect.

Acknowledgments

Thanks to Avneet Sood and Clell J. (C.J.) Solomon for providing some of the MCNP input files and insights into detector calculations.

Appendix A: Complete Listing of Result Plots

In addition to the plots not provided in the main text, larger versions of the figures in the text are included in this appendix. Fig. 6 contains larger versions of the PDF versus CDF sampling problems, the ball problems span Figs. 7 to 36, the photon backscatter problems span Figs. 37 to 46, Fig. 47 is a larger version of the SiLi detector plots, and Fig. 48 is a larger version of the Ge detector plots.

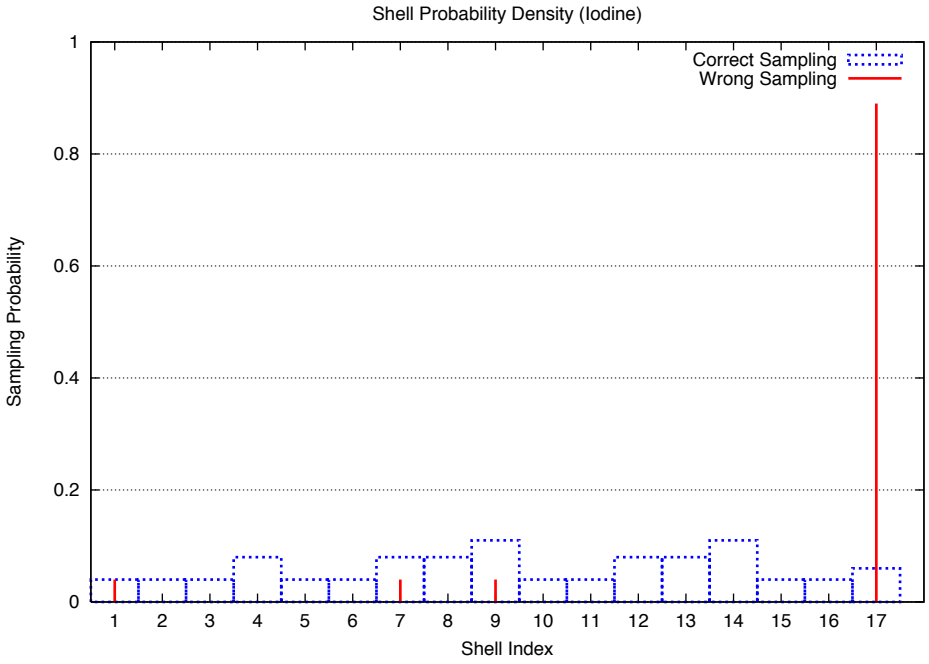

(a)

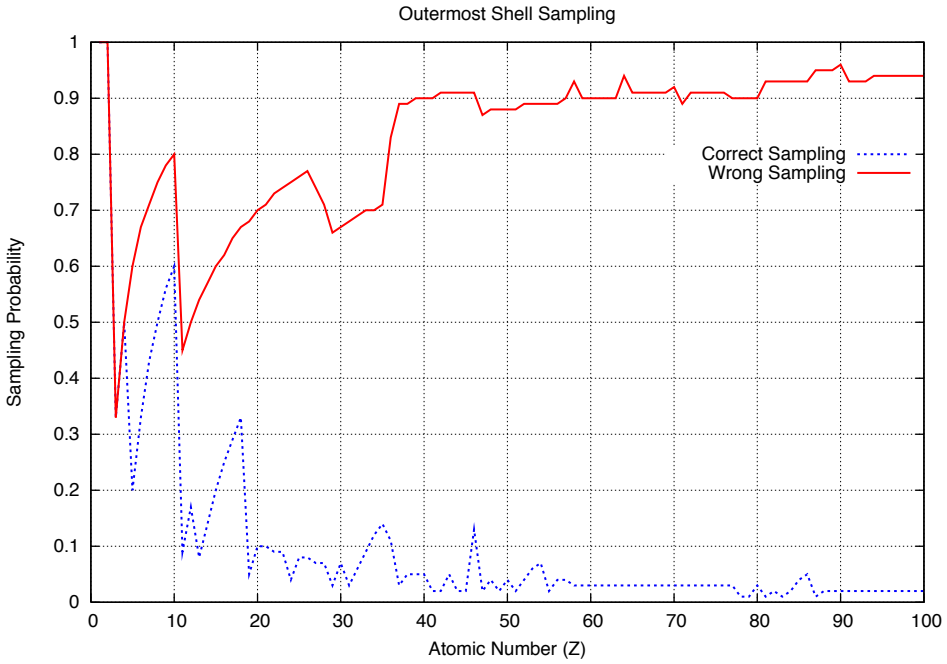

(b)

Figure 6: (a) Sampling of shells for iodine. (b) Outermost shell sampling probabilities.

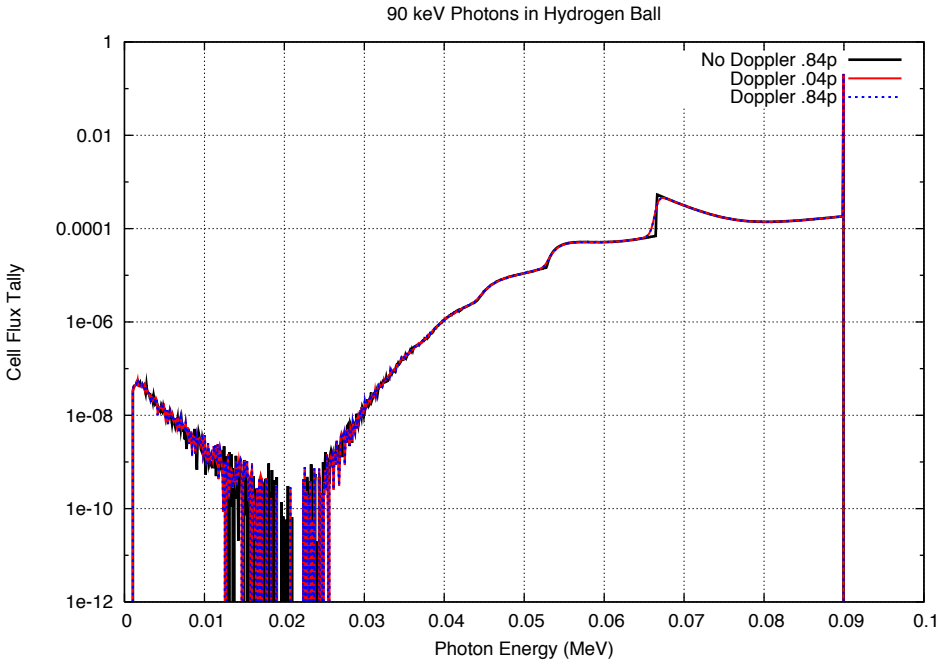

(a)

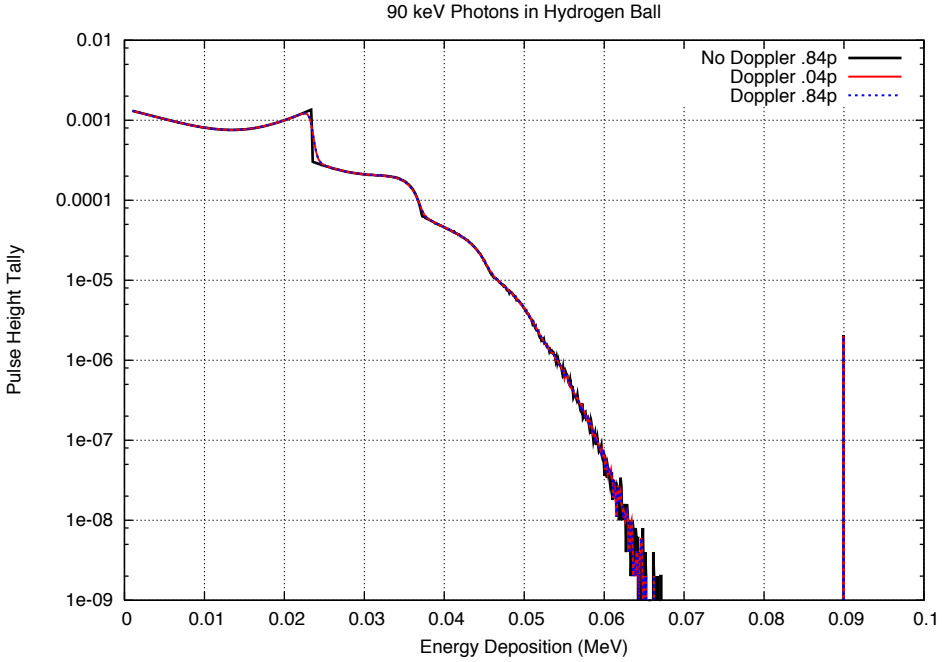

(b)

Figure 7: Cell flux (a) and energy deposition (b) tallies in a Hydrogen ball.

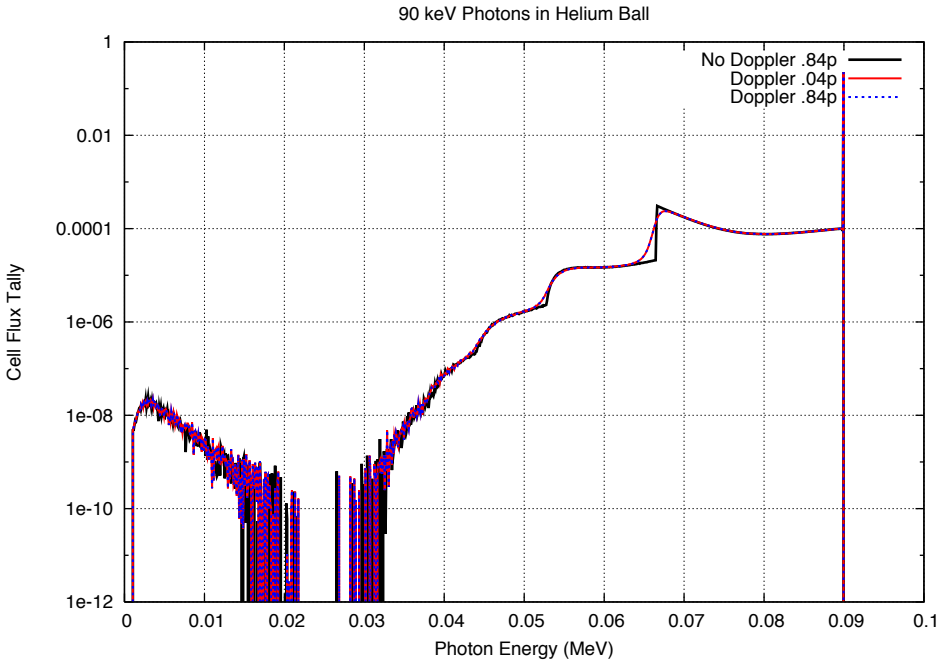

(a)

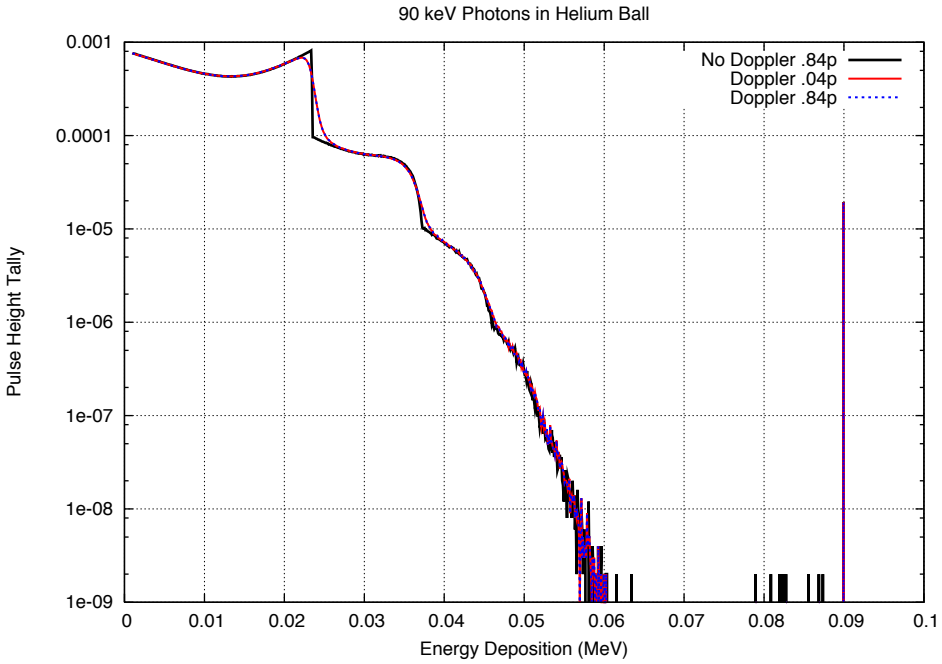

(b)

Figure 8: Cell flux (a) and energy deposition (b) tallies in a Helium ball.

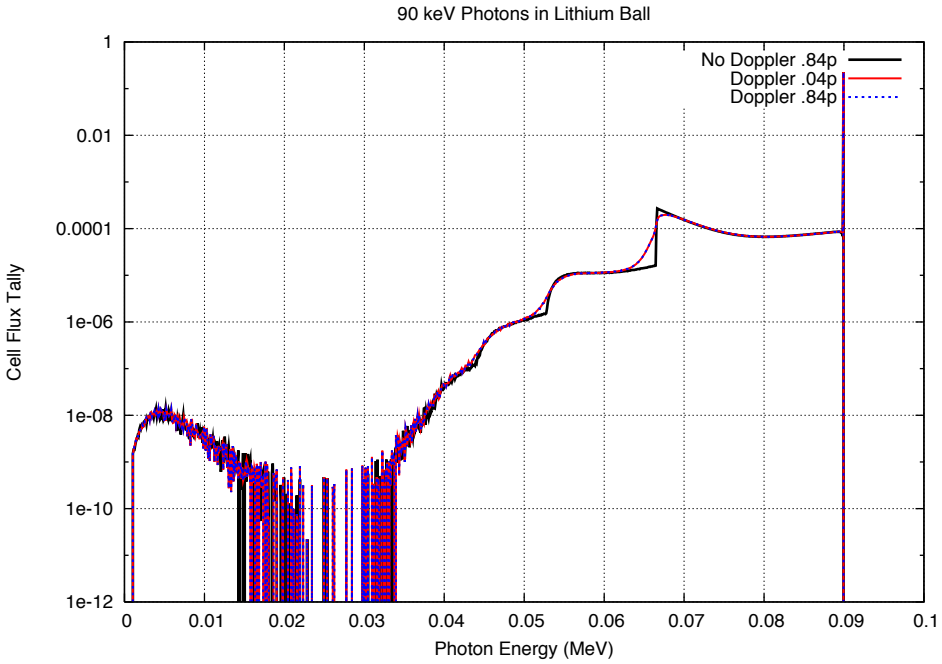

(a)

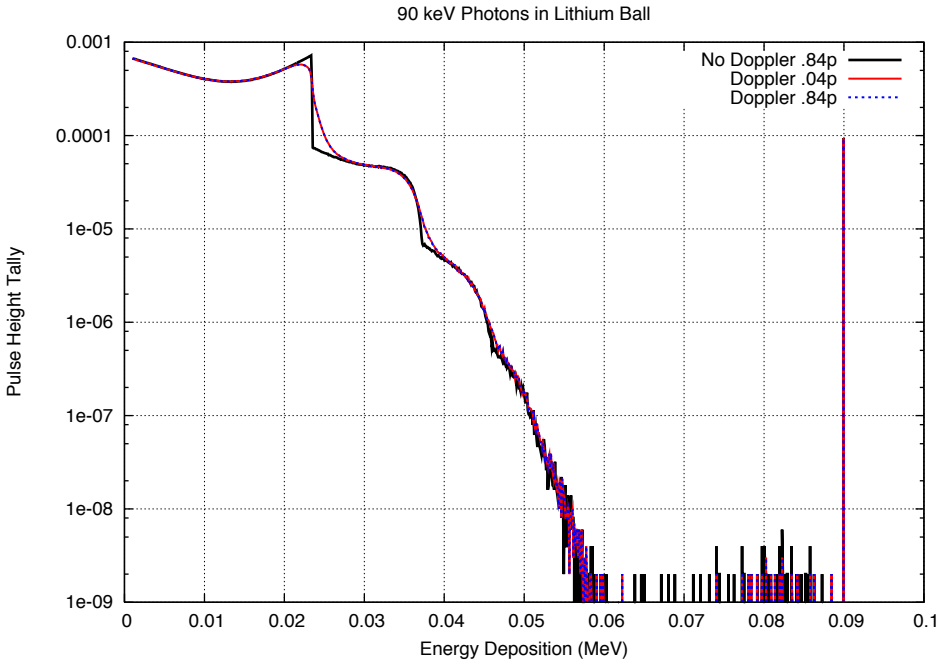

(b)

Figure 9: Cell flux (a) and energy deposition (b) tallies in a Lithium ball.

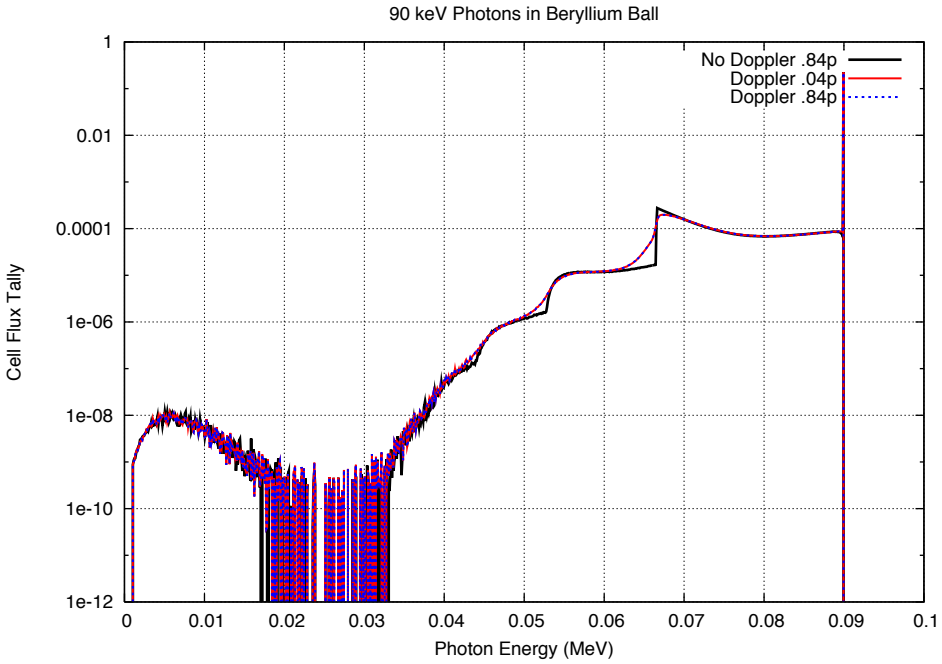

(a)

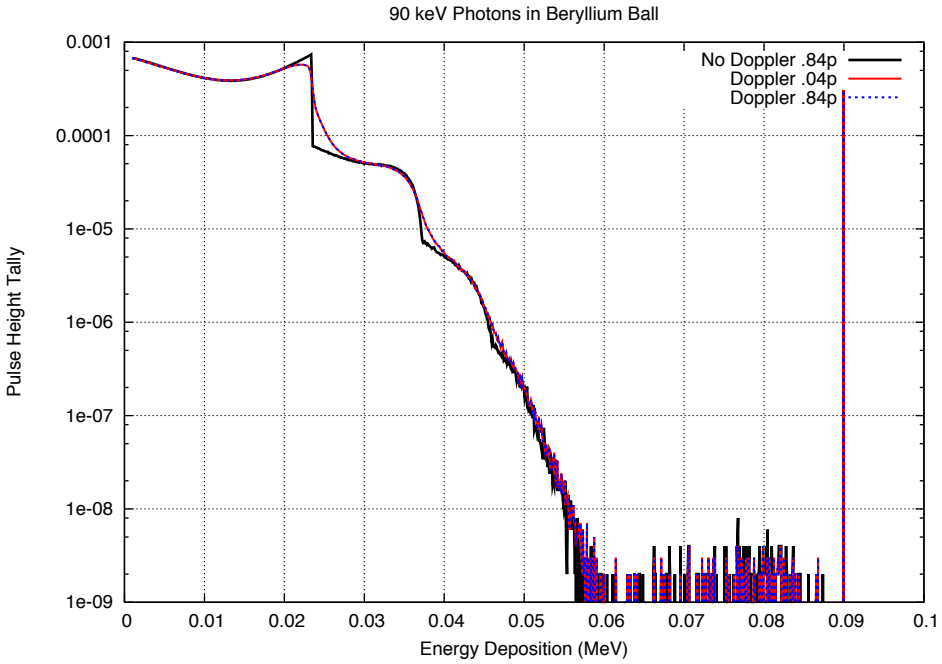

(b)

Figure 10: Cell flux (a) and energy deposition (b) tallies in a Beryllium ball.

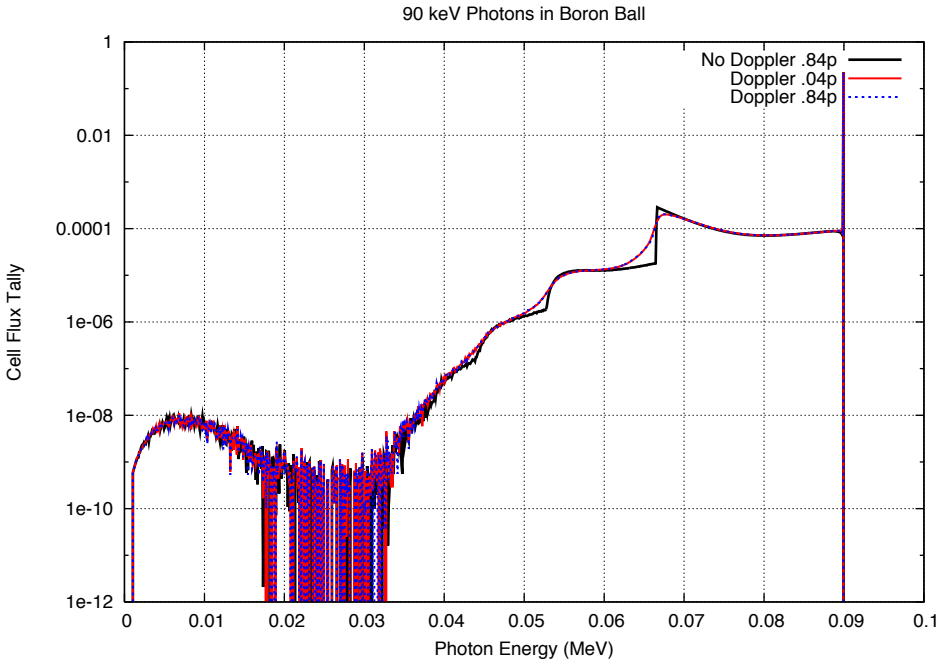

(a)

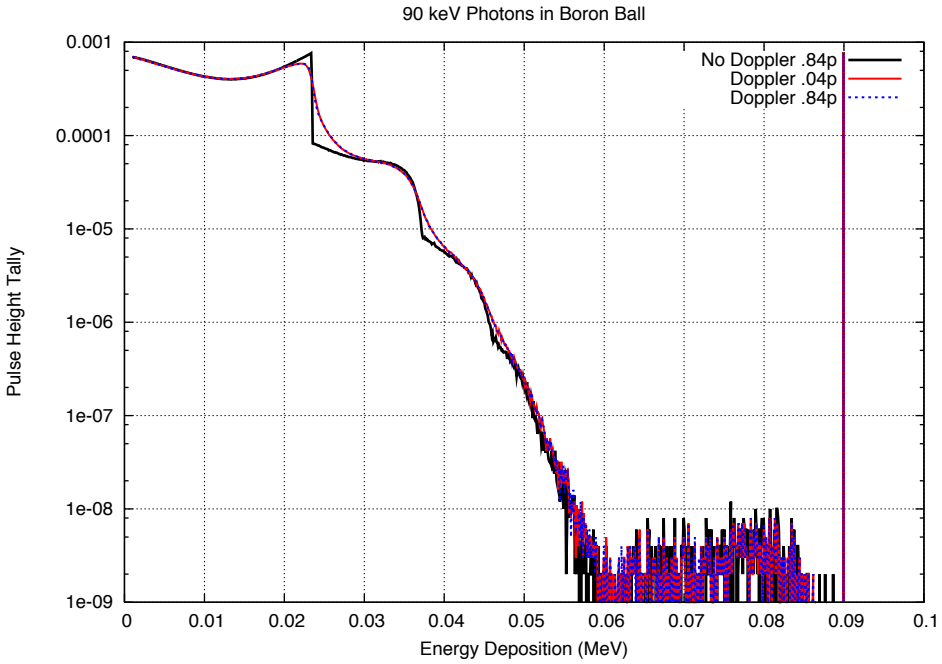

(b)

Figure 11: Cell flux (a) and energy deposition (b) tallies in a Boron ball.

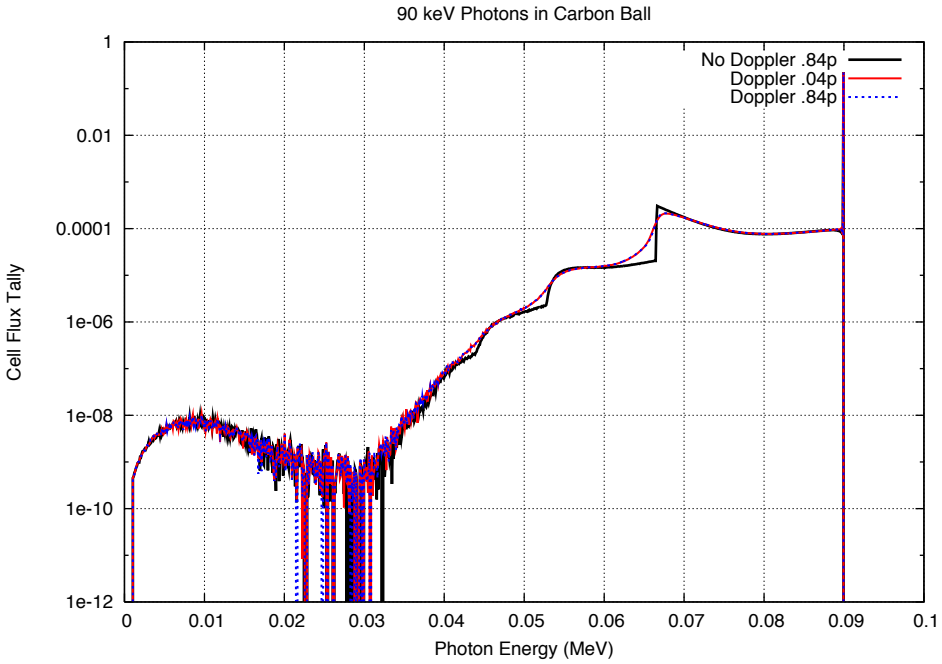

(a)

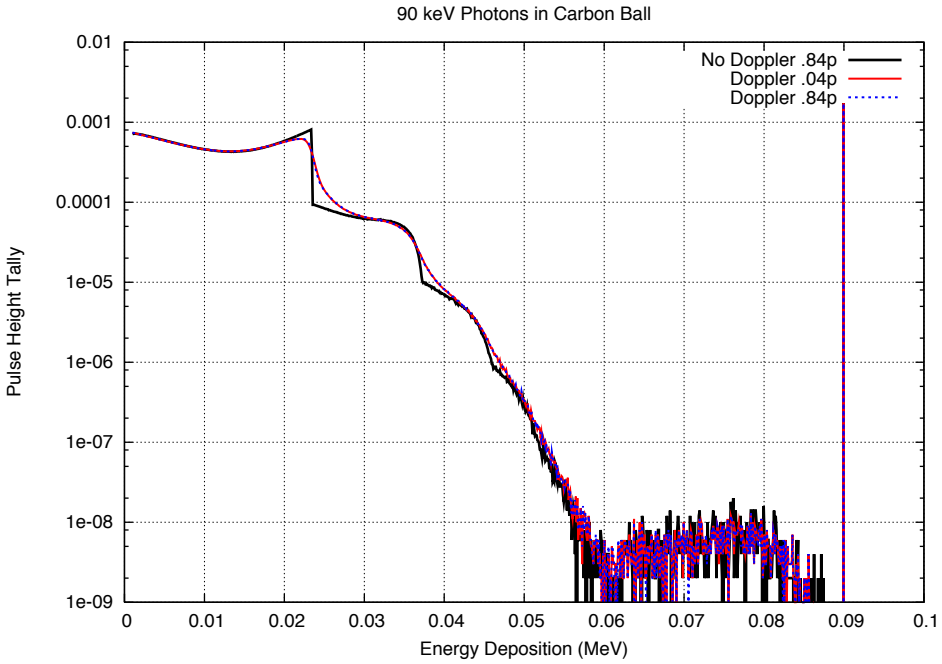

(b)

Figure 12: Cell flux (a) and energy deposition (b) tallies in a Carbon ball.

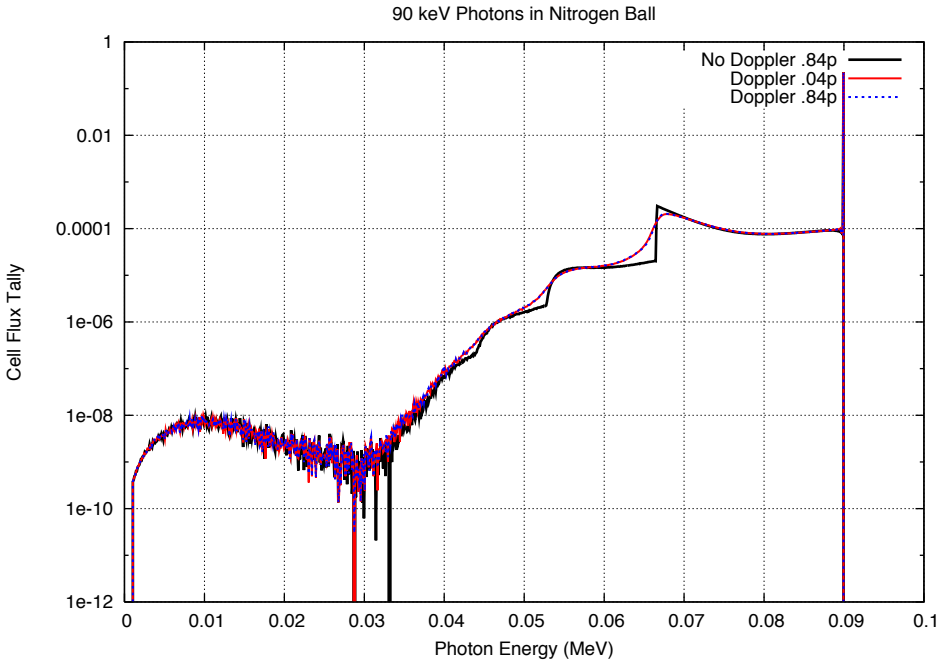

(a)

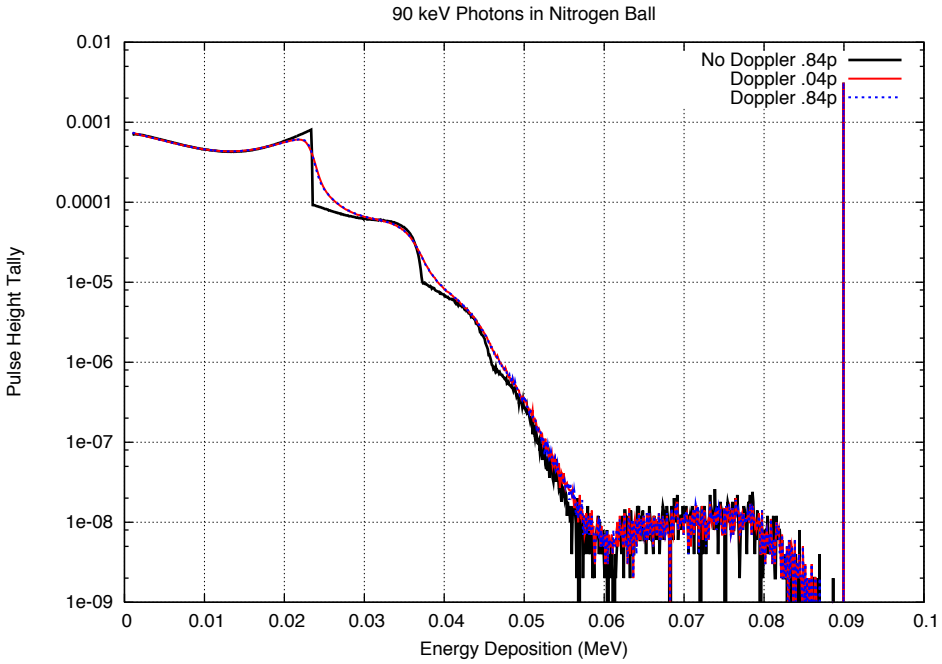

(b)

Figure 13: Cell flux (a) and energy deposition (b) tallies in a Nitrogen ball.

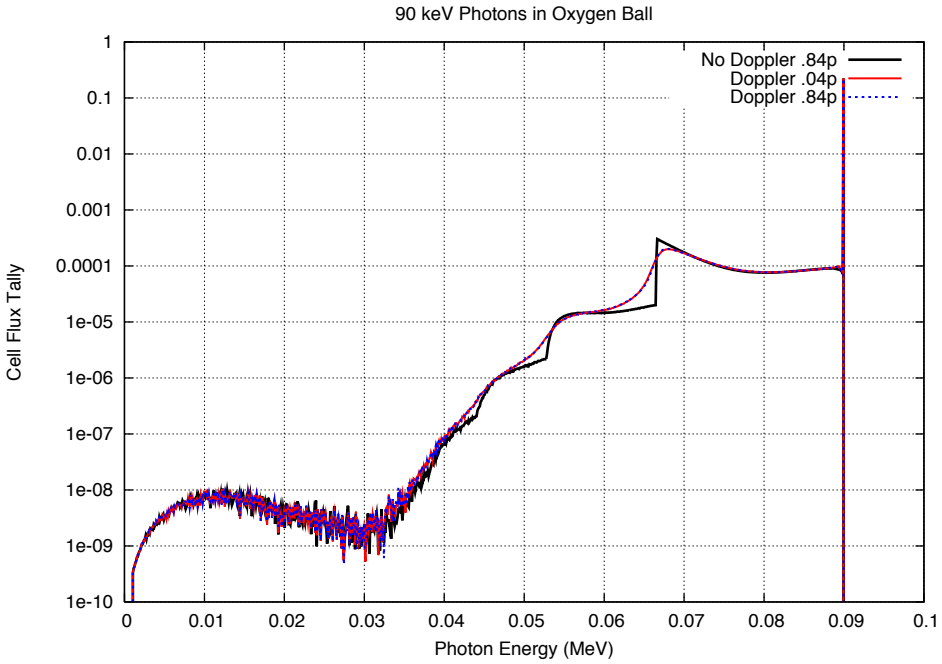

(a)

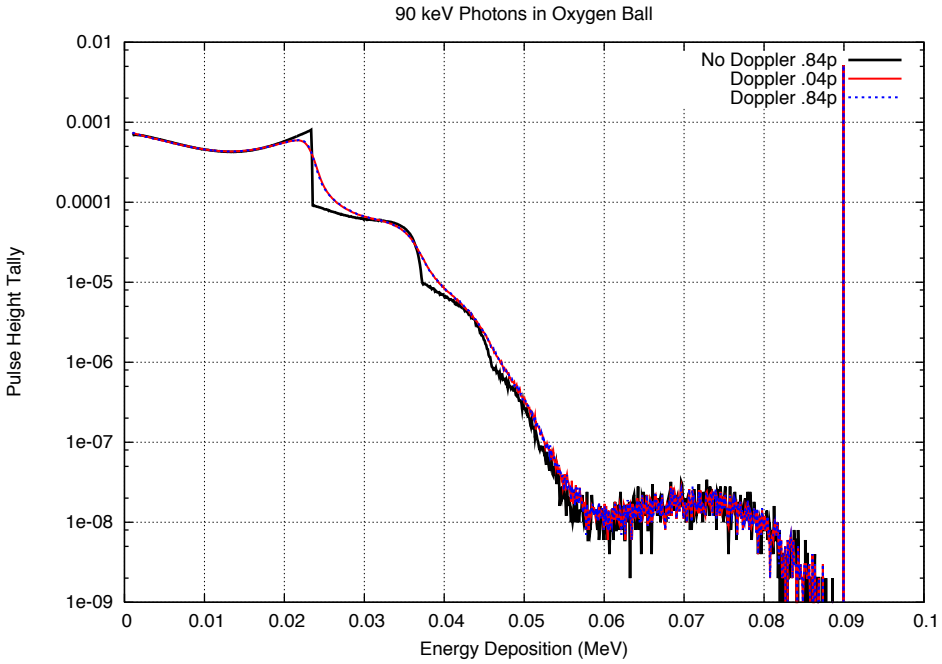

(b)

Figure 14: Cell flux (a) and energy deposition (b) tallies in a Oxygen ball.

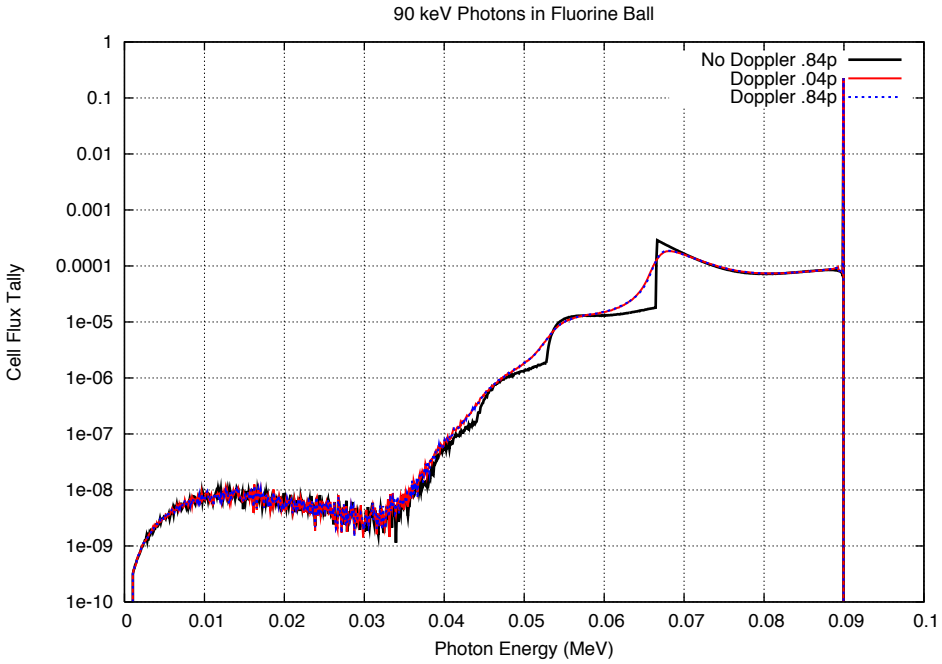

(a)

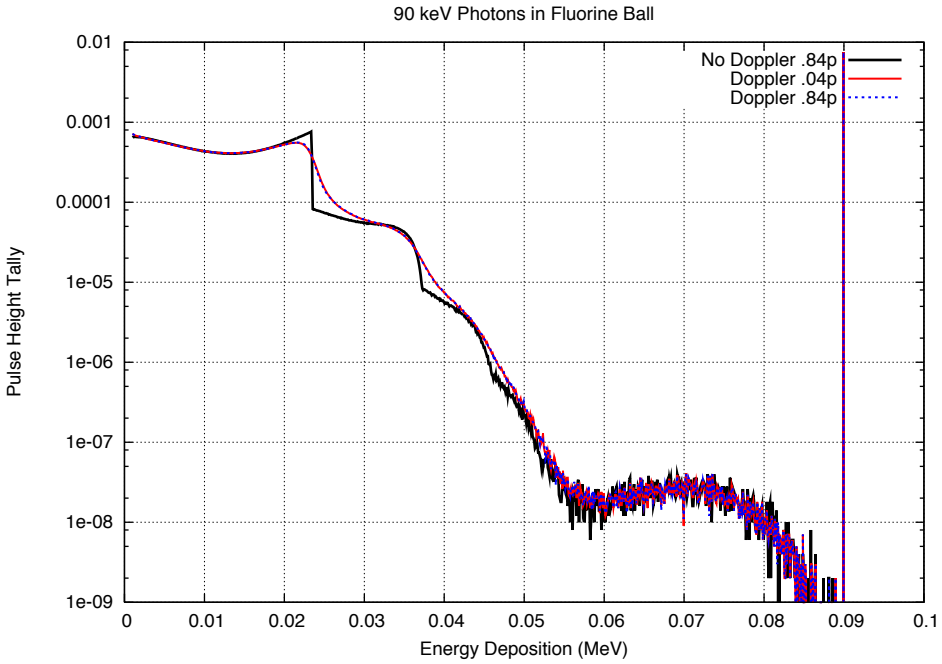

(b)

Figure 15: Cell flux (a) and energy deposition (b) tallies in a Fluorine ball.

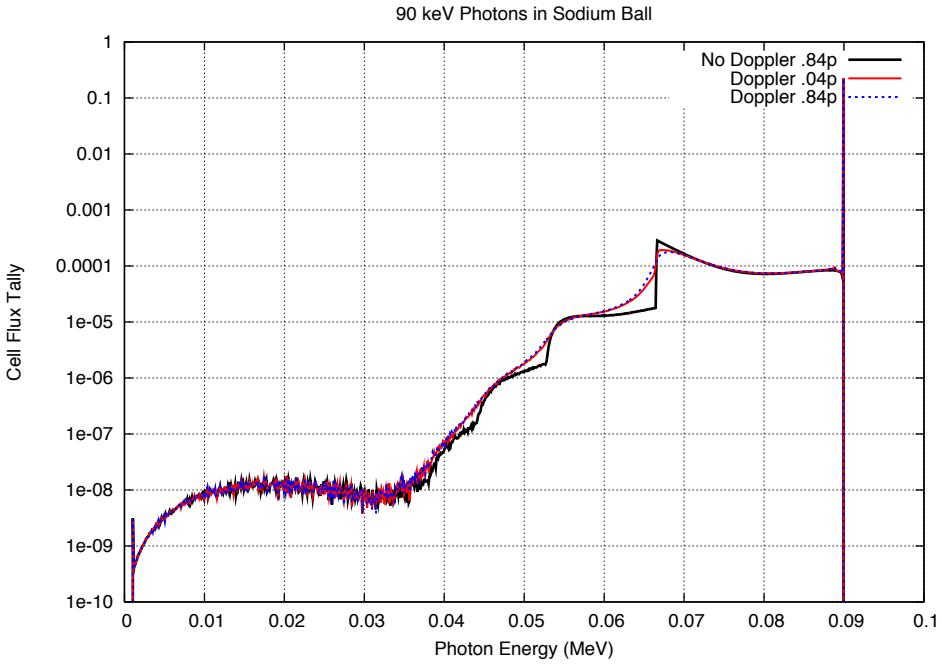

(a)

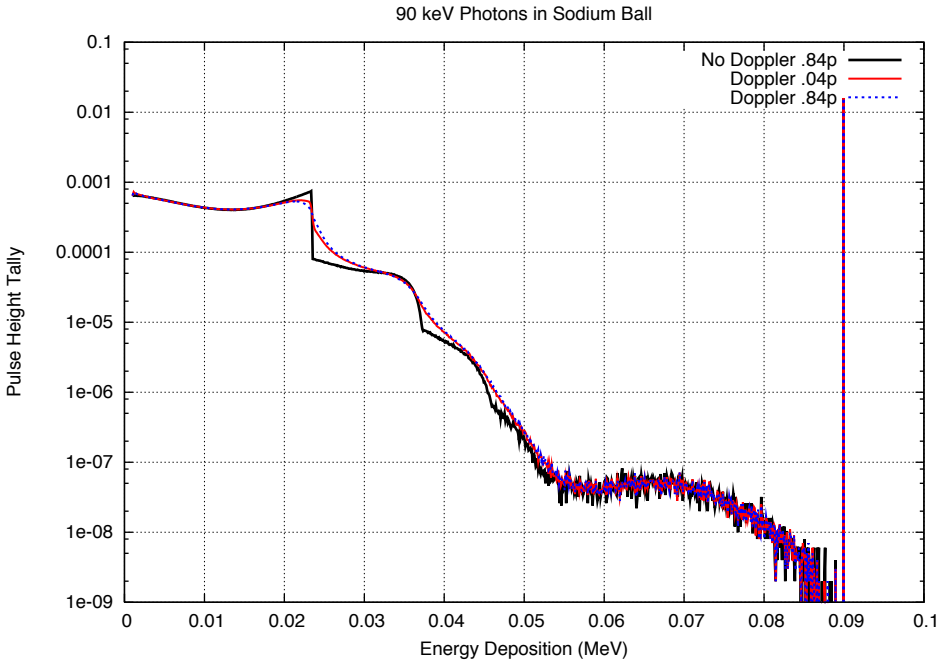

(b)

Figure 16: Cell flux (a) and energy deposition (b) tallies in a Sodium ball.

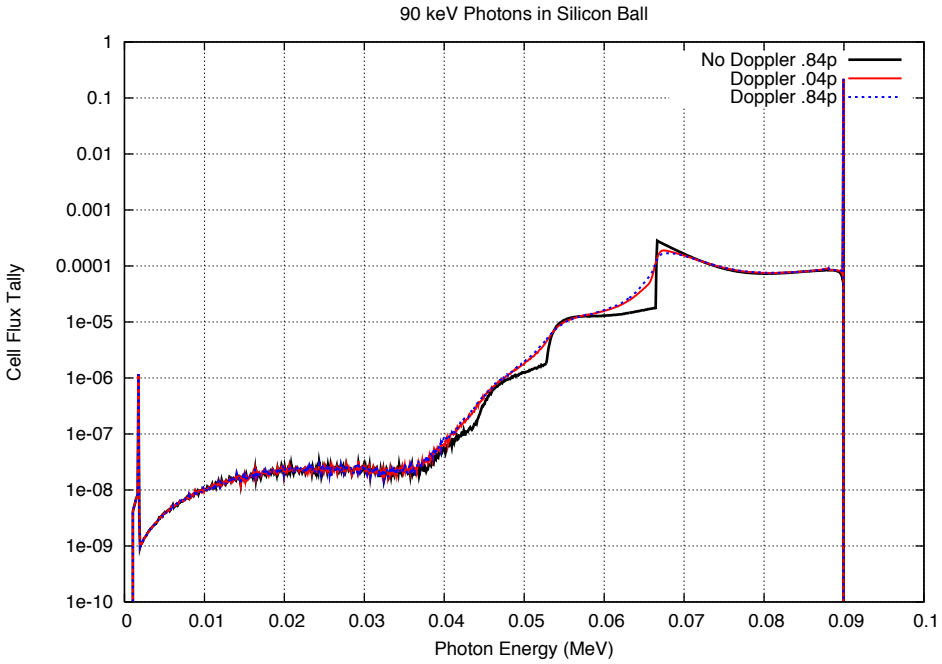

(a)

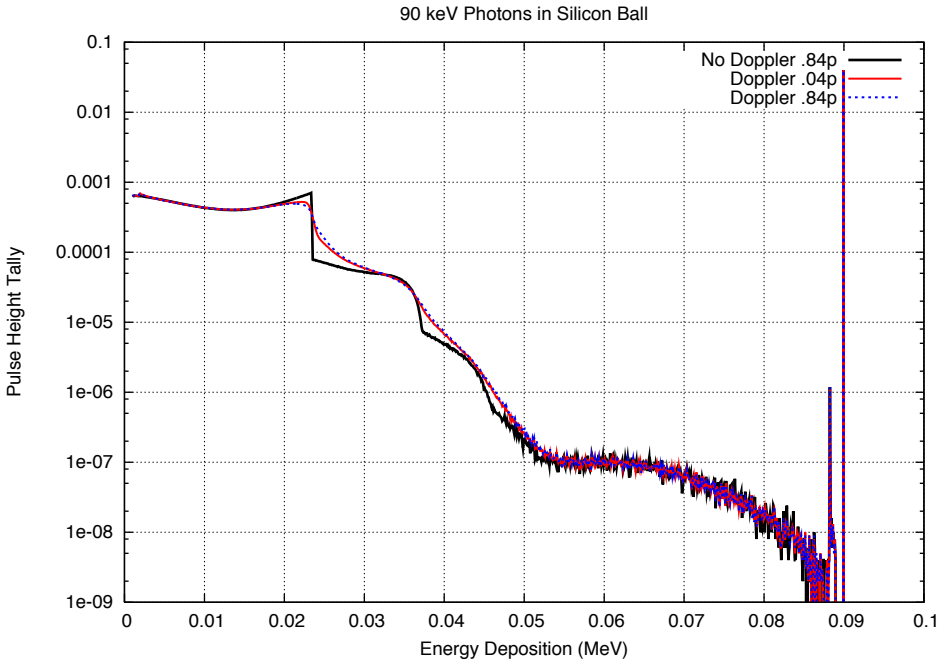

(b)

Figure 17: Cell flux (a) and energy deposition (b) tallies in a Silicon ball.

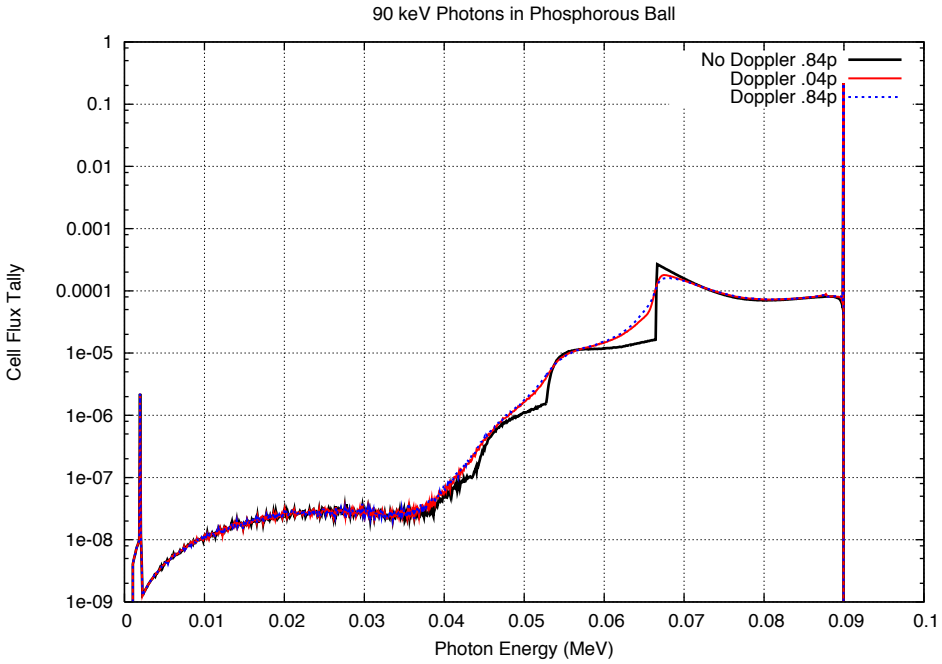

(a)

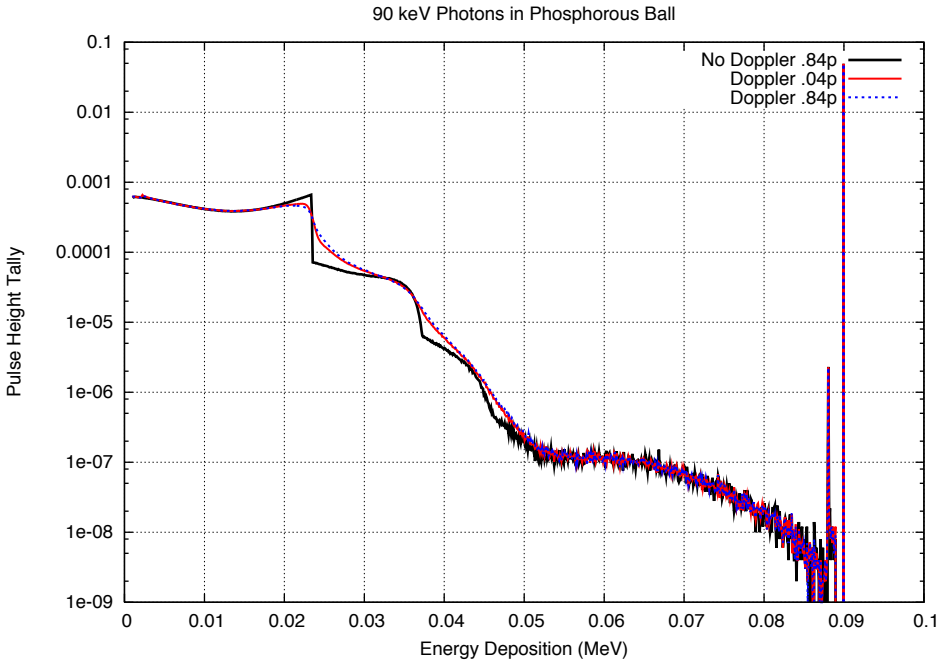

(b)

Figure 18: Cell flux (a) and energy deposition (b) tallies in a Phosphorous ball.

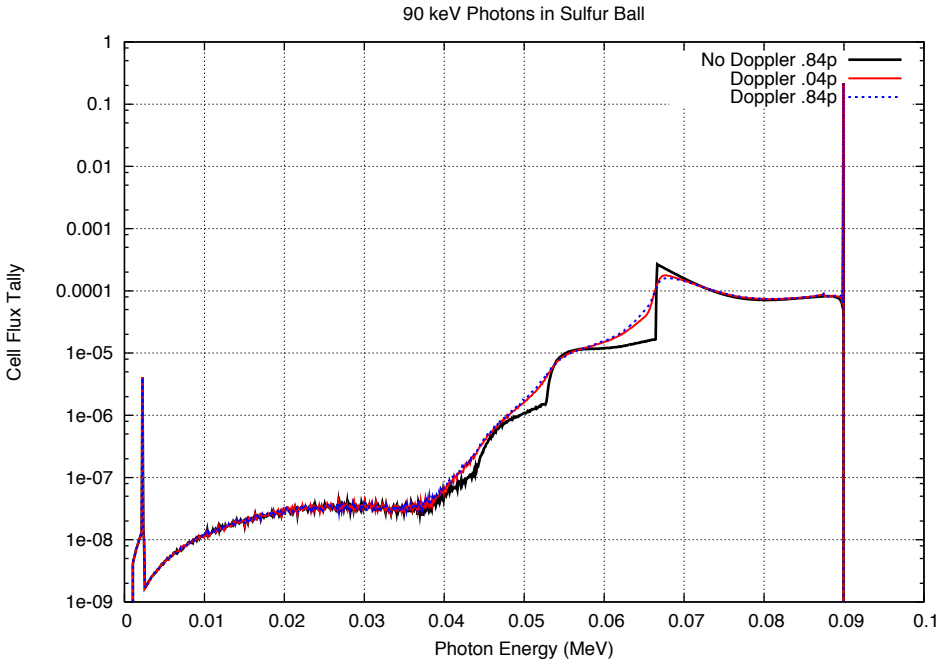

(a)

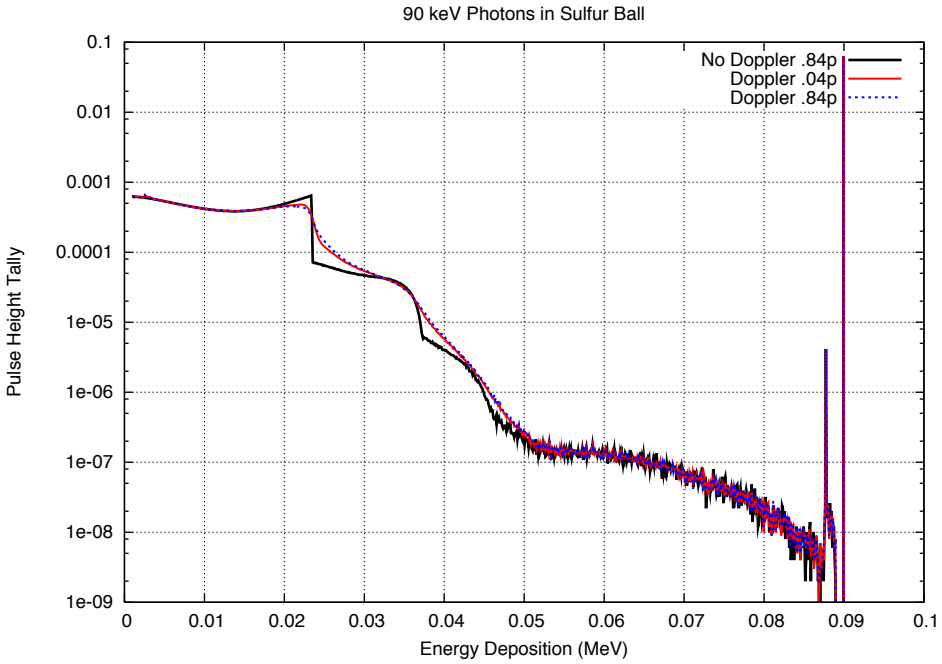

(b)

Figure 19: Cell flux (a) and energy deposition (b) tallies in a Sulfur ball.

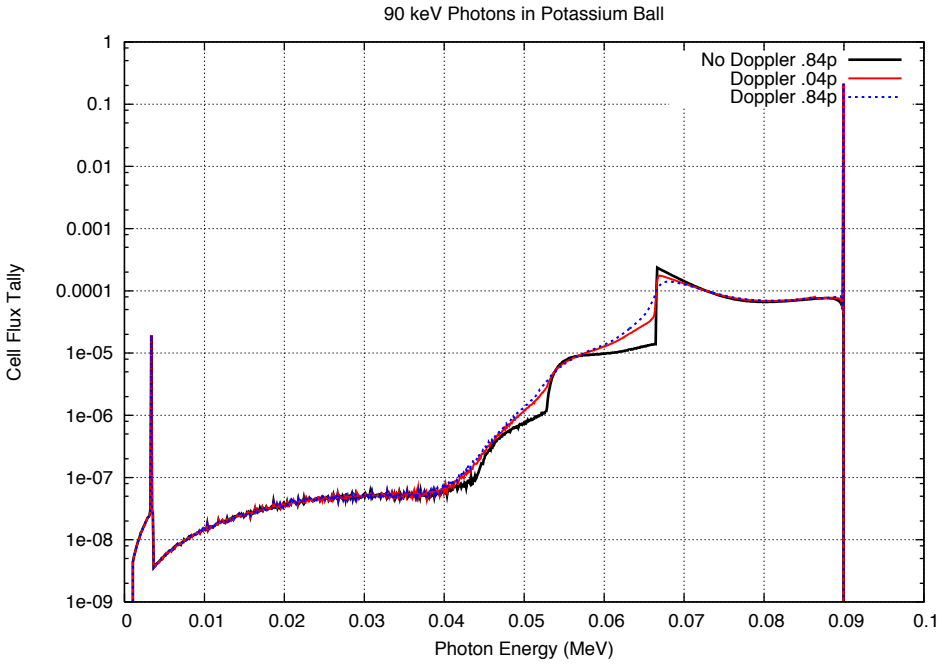

(a)

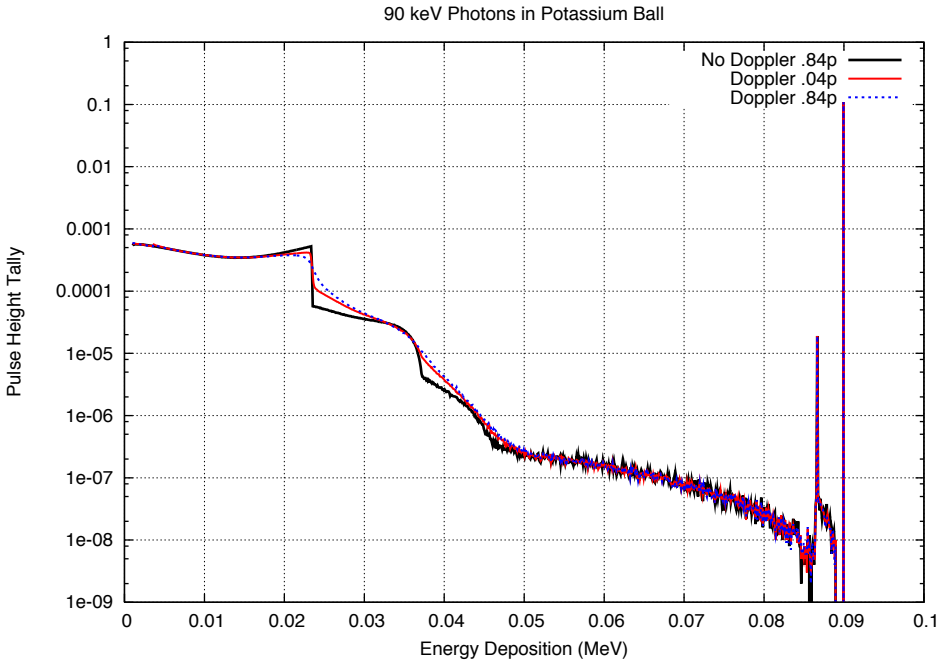

(b)

Figure 20: Cell flux (a) and energy deposition (b) tallies in a Potassium ball.

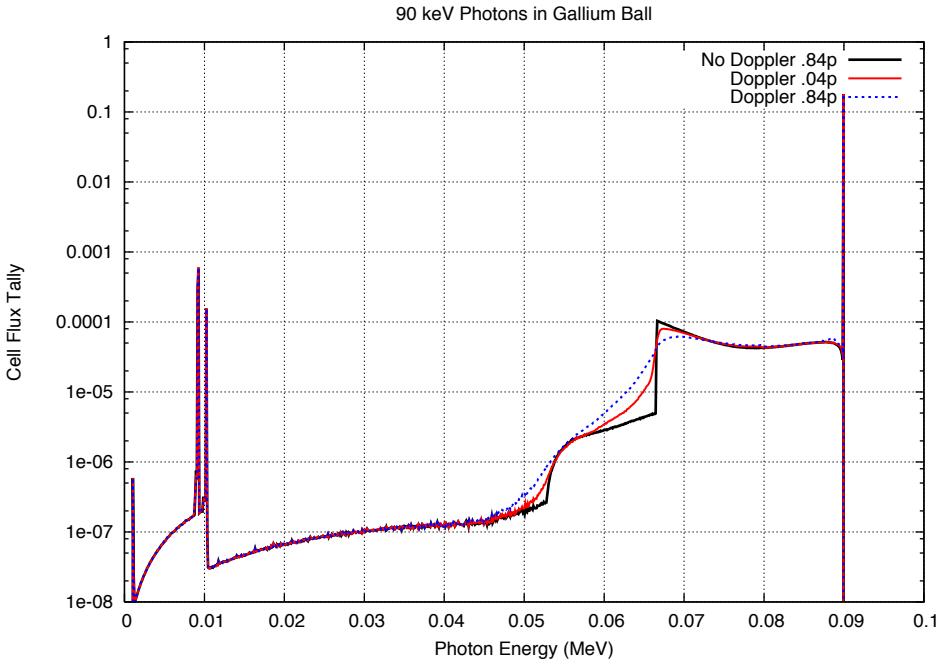

(a)

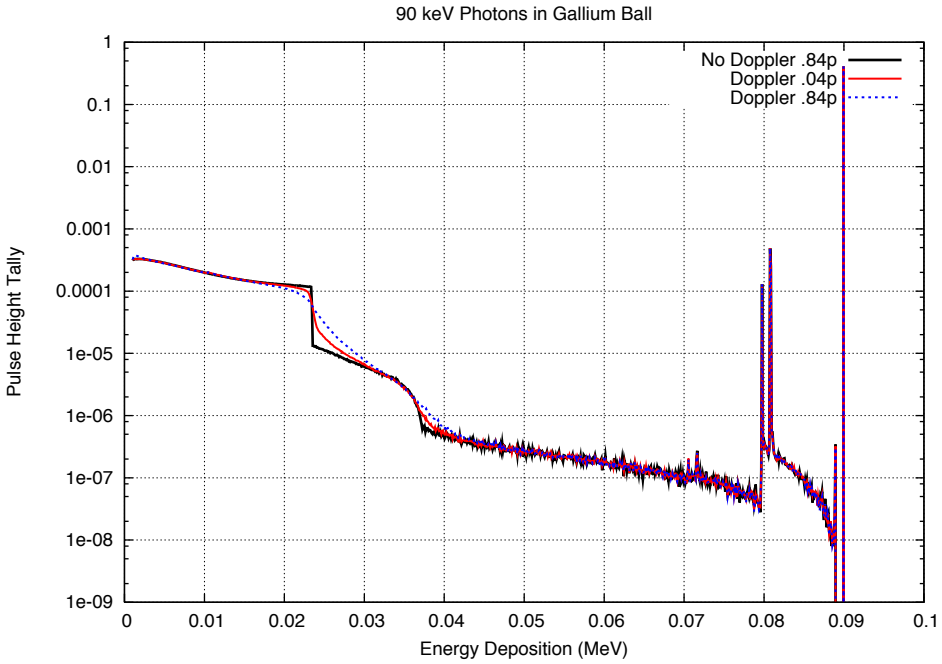

(b)

Figure 21: Cell flux (a) and energy deposition (b) tallies in a Gallium ball.

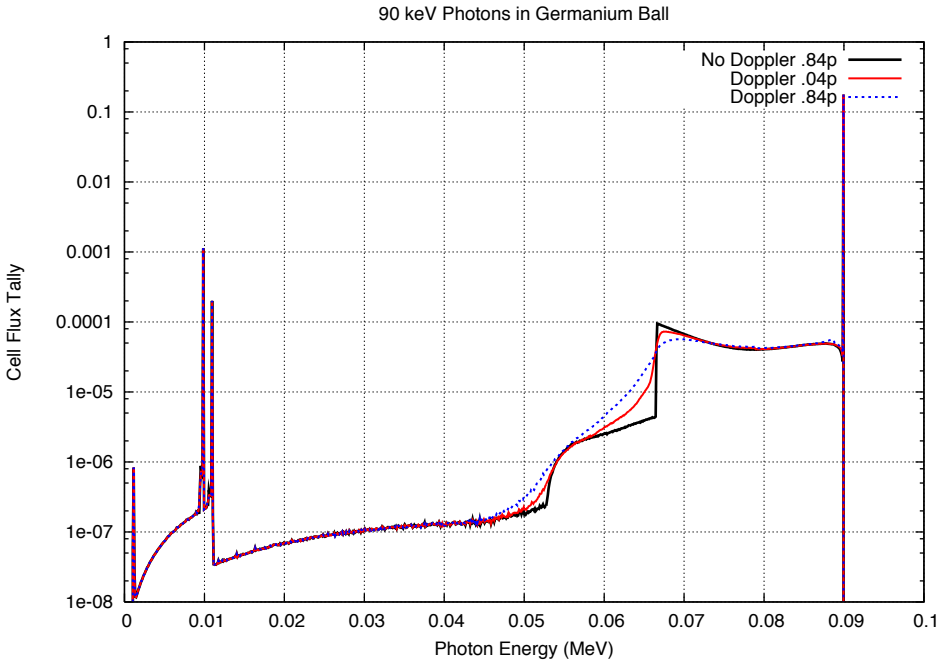

(a)

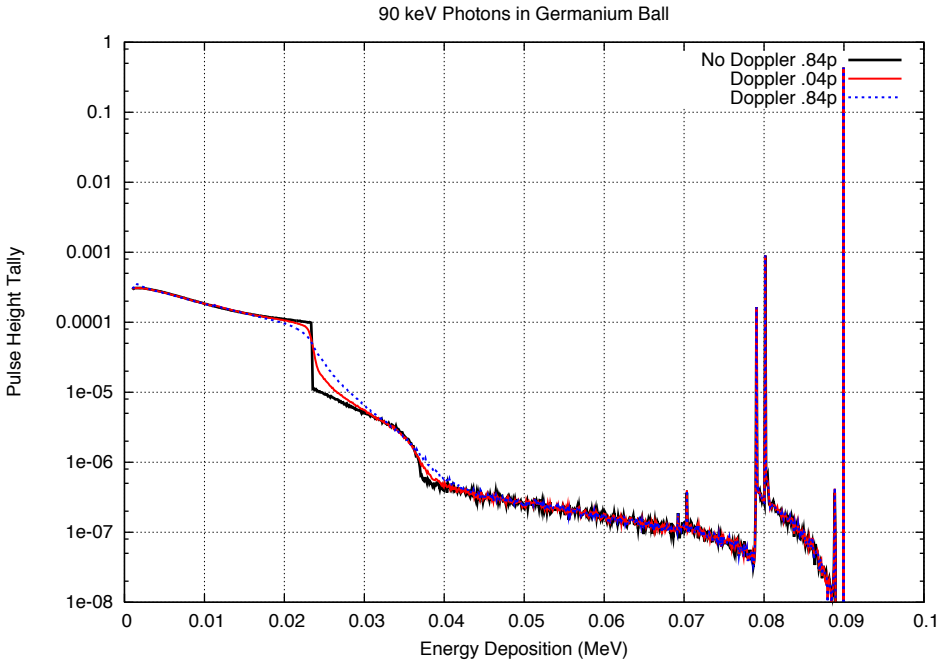

(b)

Figure 22: Cell flux (a) and energy deposition (b) tallies in a Germanium ball.

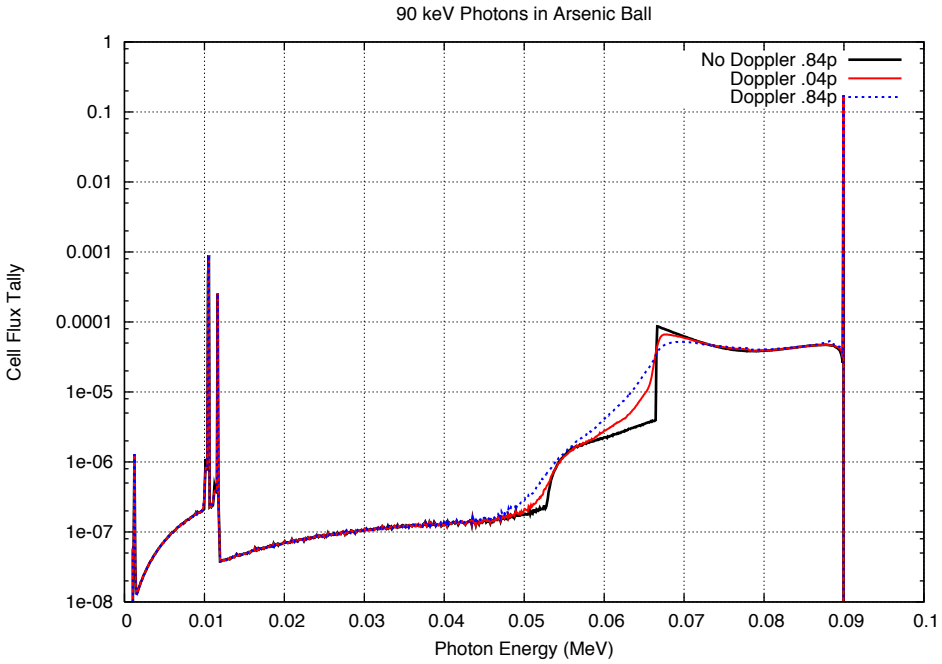

(a)

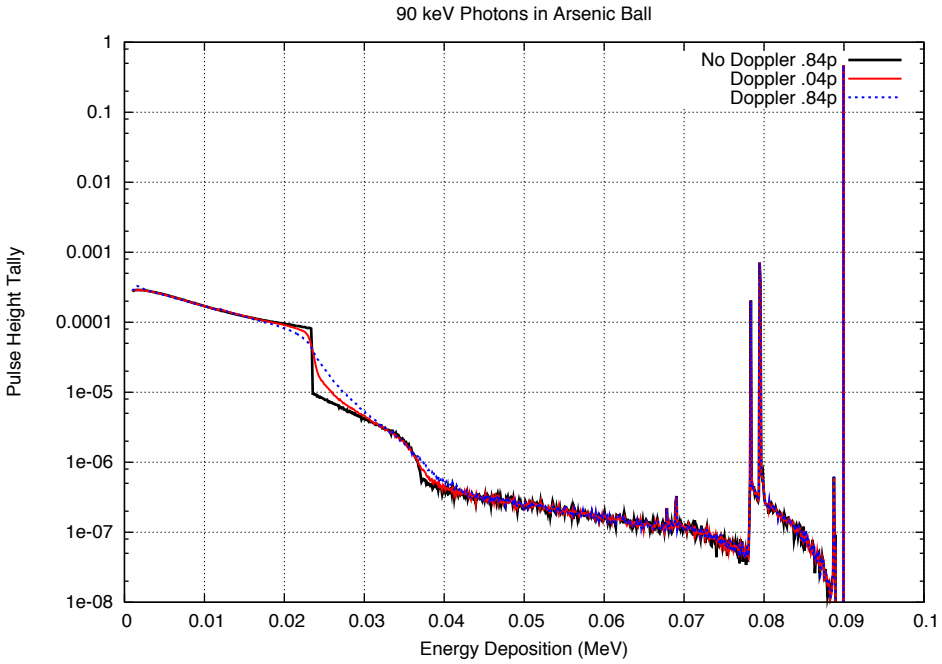

(b)

Figure 23: Cell flux (a) and energy deposition (b) tallies in a Arsenic ball.

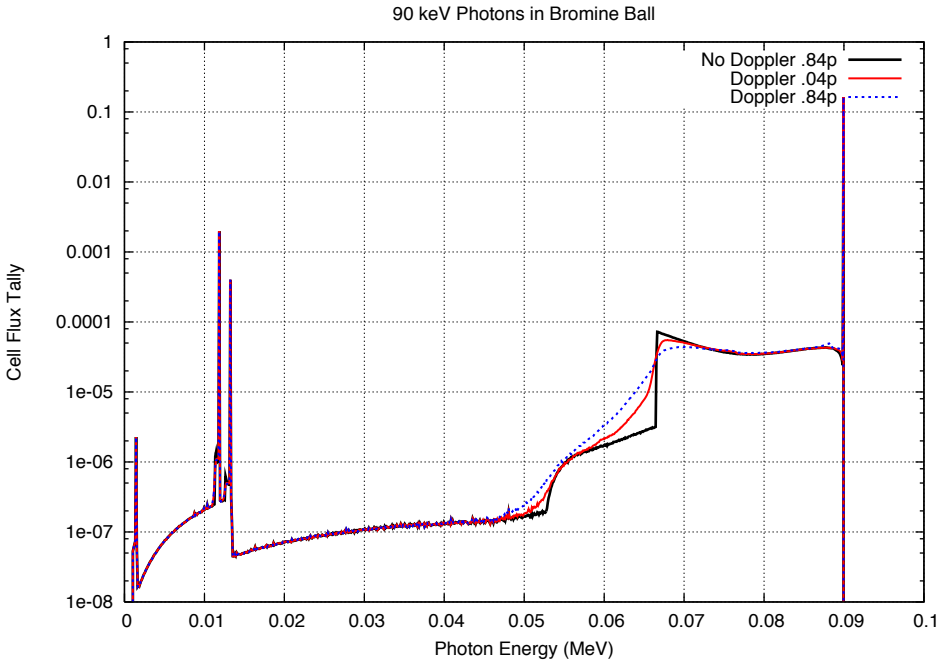

(a)

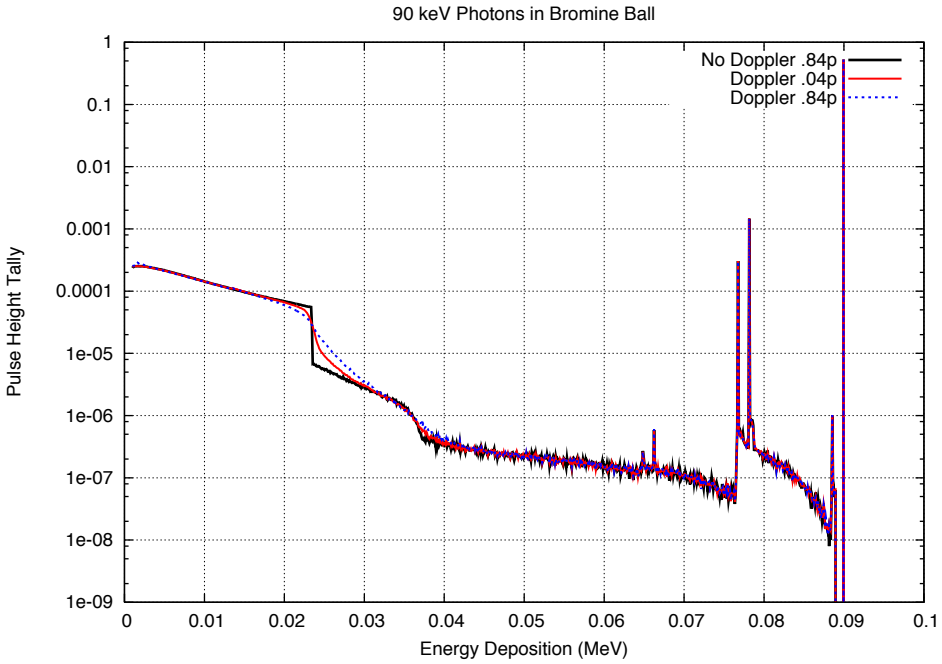

(b)

Figure 24: Cell flux (a) and energy deposition (b) tallies in a Bromine ball.

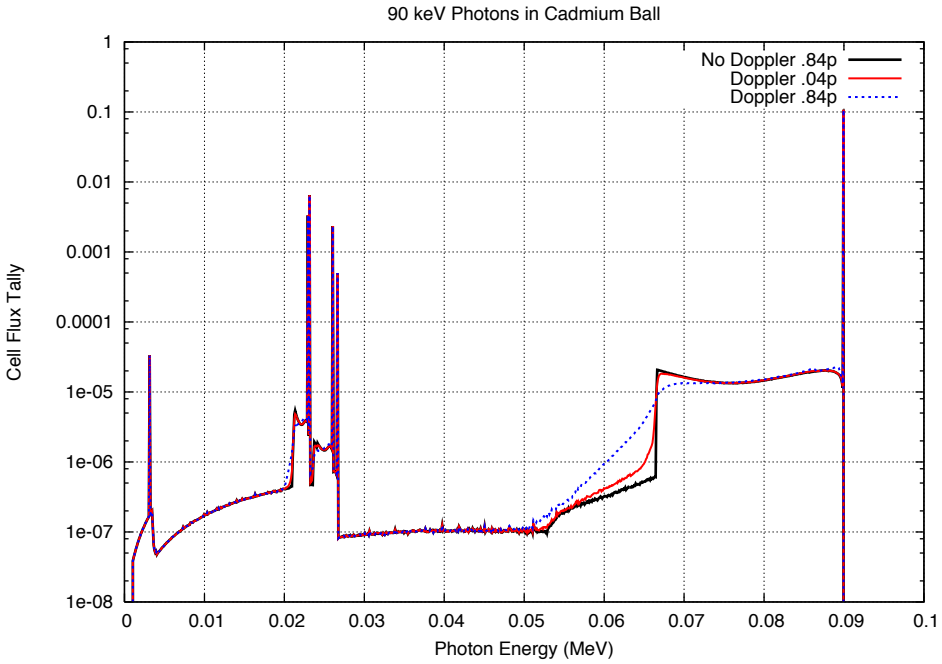

(a)

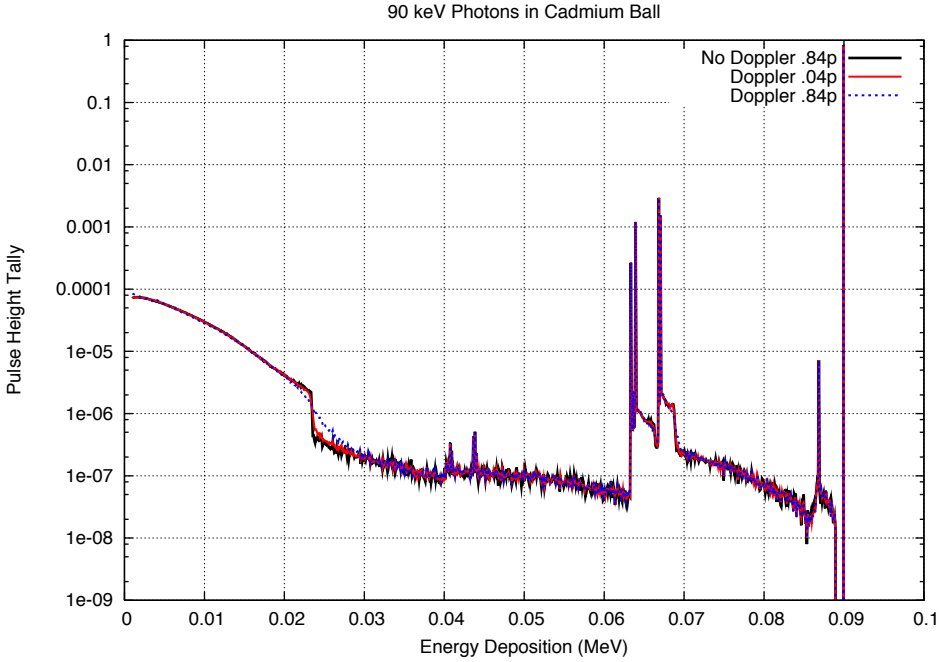

(b)

Figure 25: Cell flux (a) and energy deposition (b) tallies in a Cadmium ball.

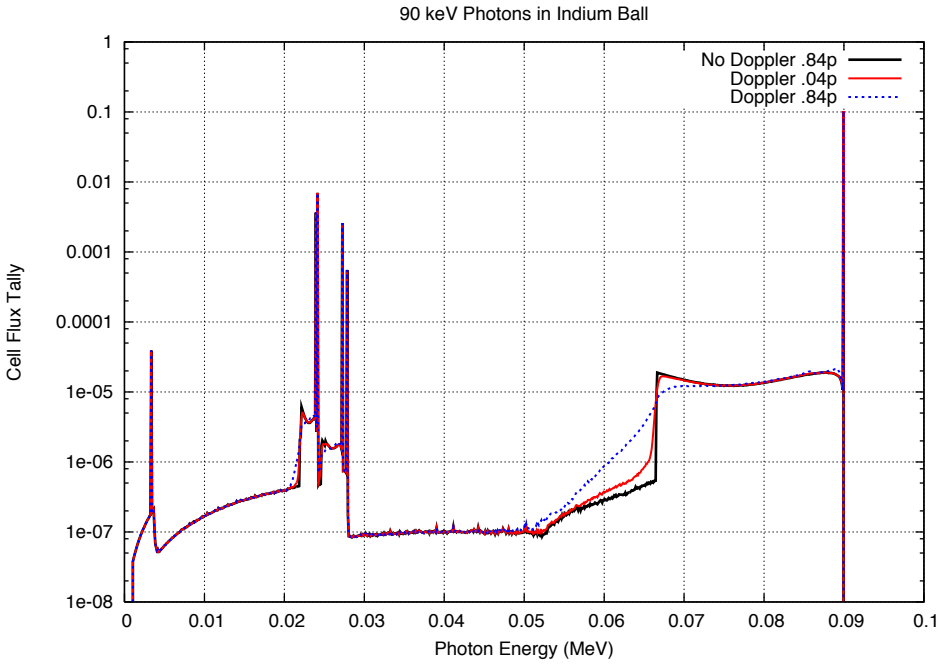

(a)

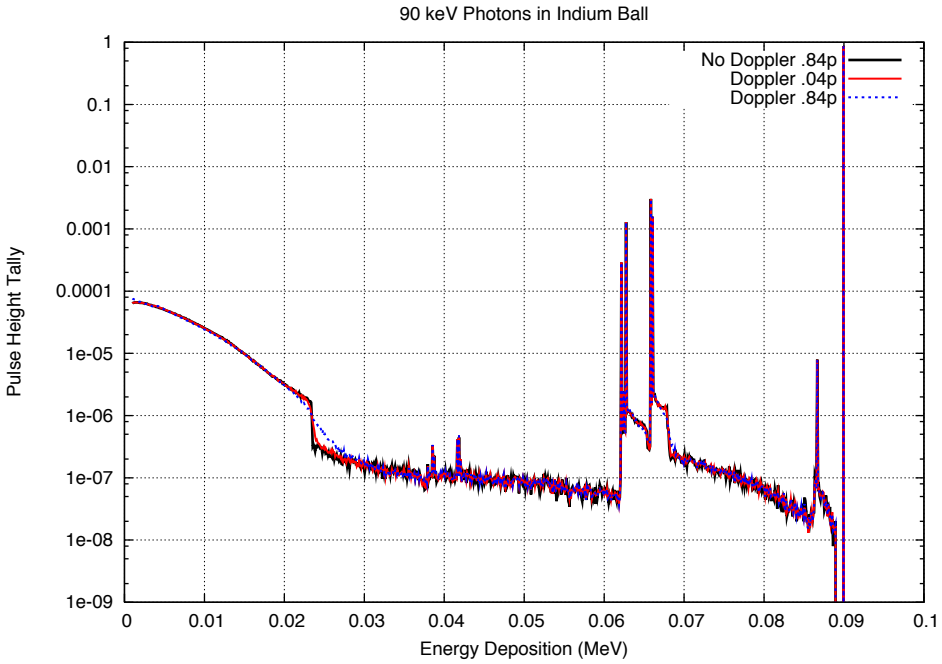

(b)

Figure 26: Cell flux (a) and energy deposition (b) tallies in a Indium ball.

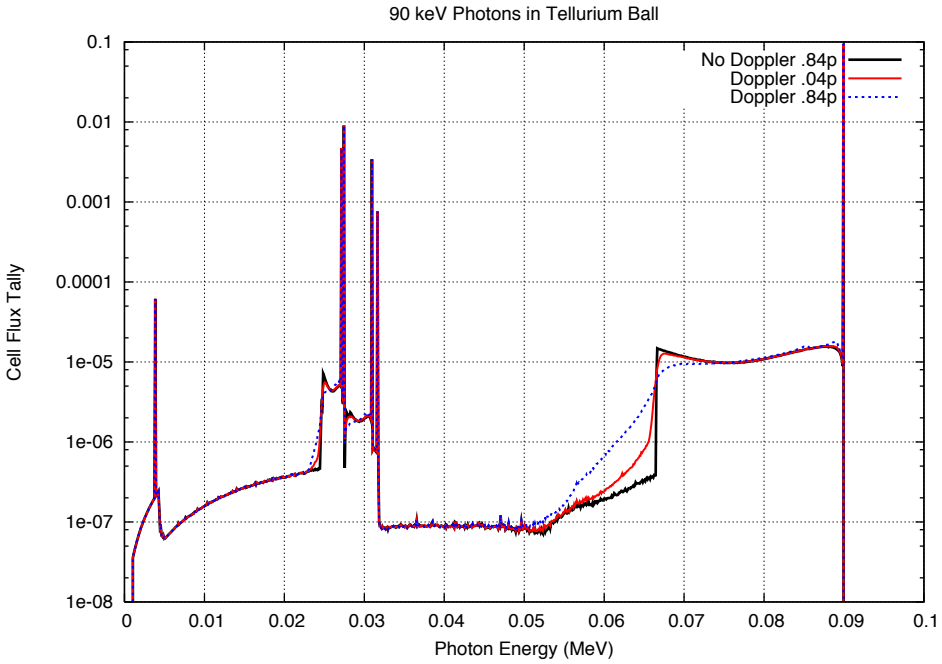

(a)

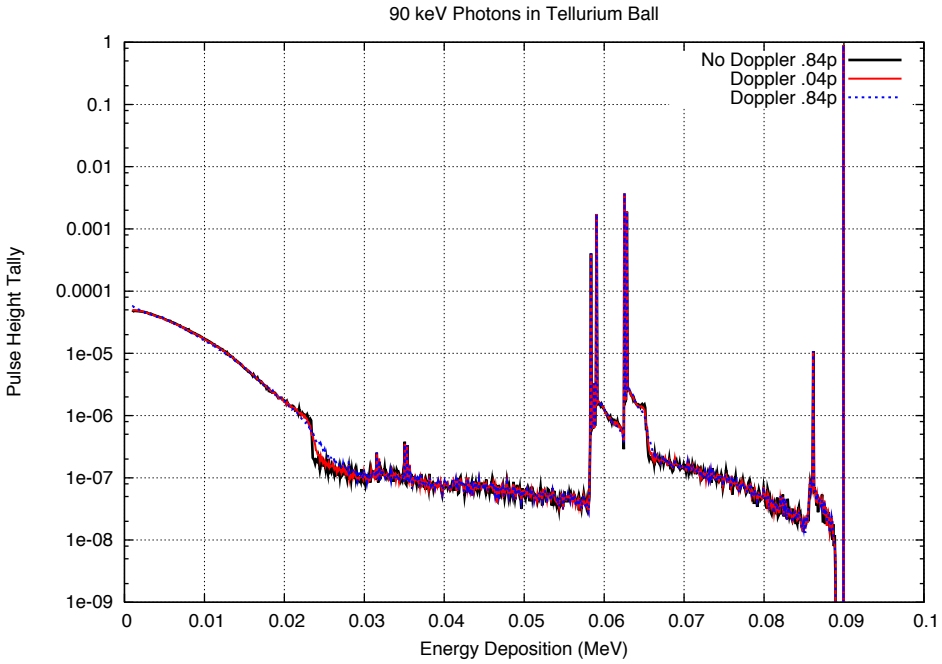

(b)

Figure 27: Cell flux (a) and energy deposition (b) tallies in a Tellurium ball.

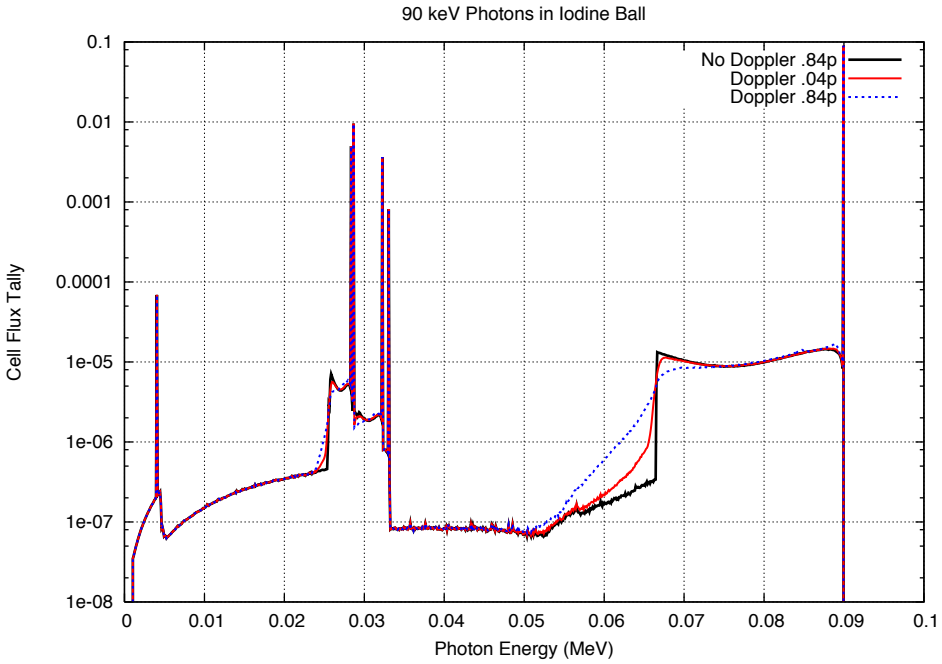

(a)

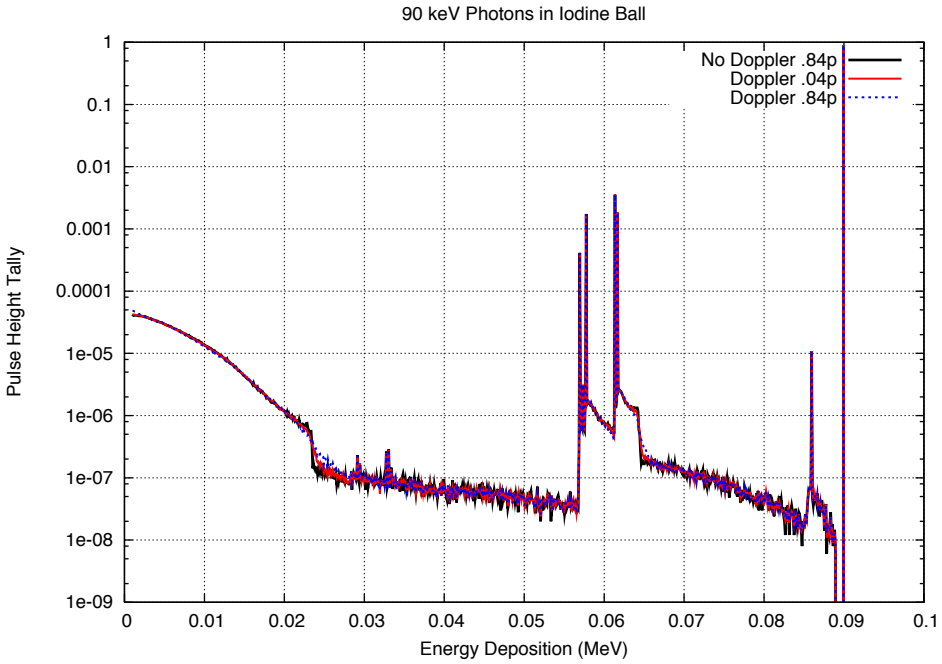

(b)

Figure 28: Cell flux (a) and energy deposition (b) tallies in a Iodine ball.

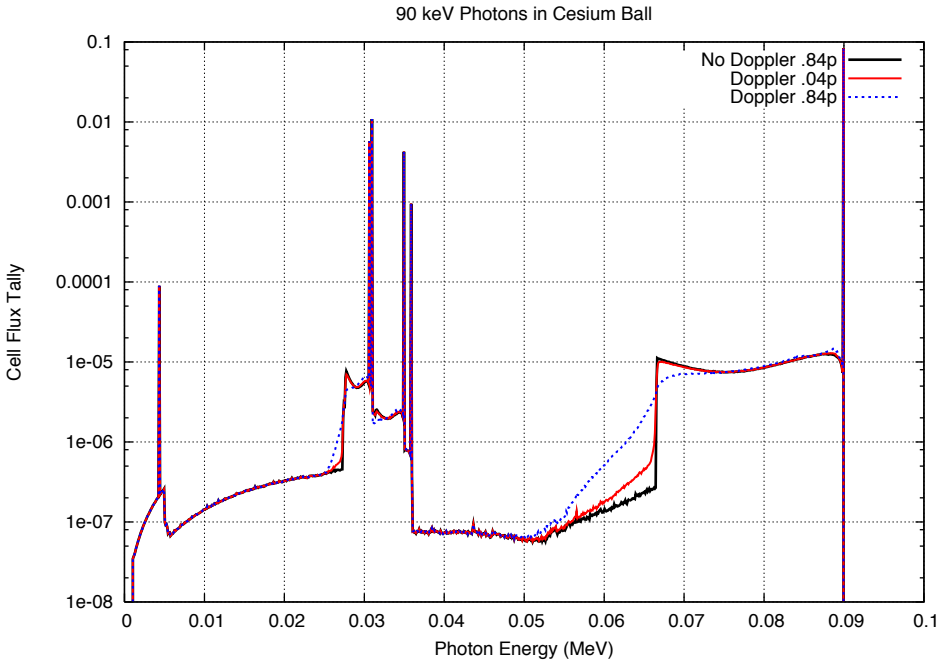

(a)

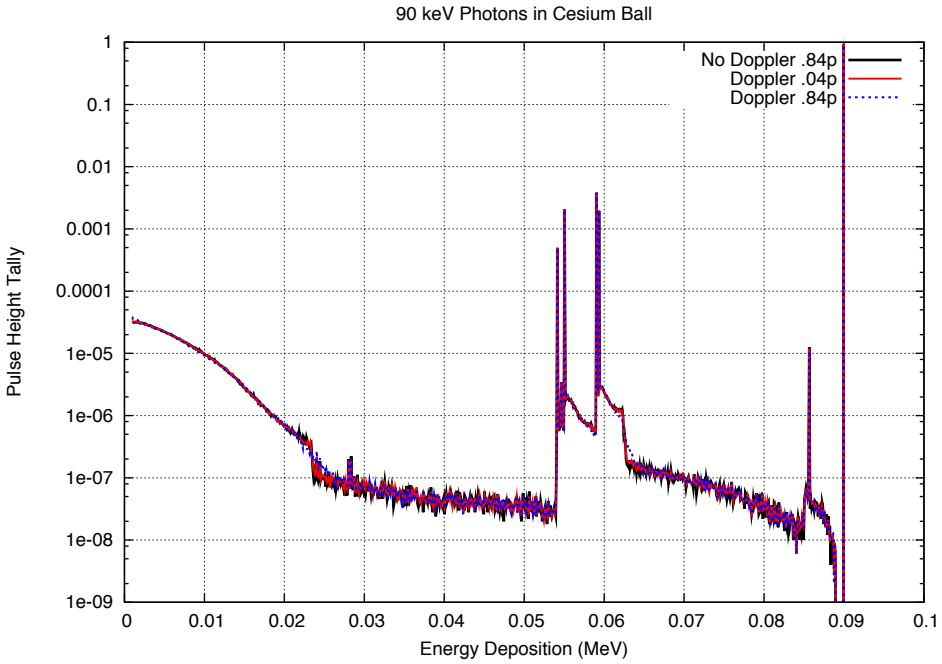

(b)

Figure 29: Cell flux (a) and energy deposition (b) tallies in a Cesium ball.

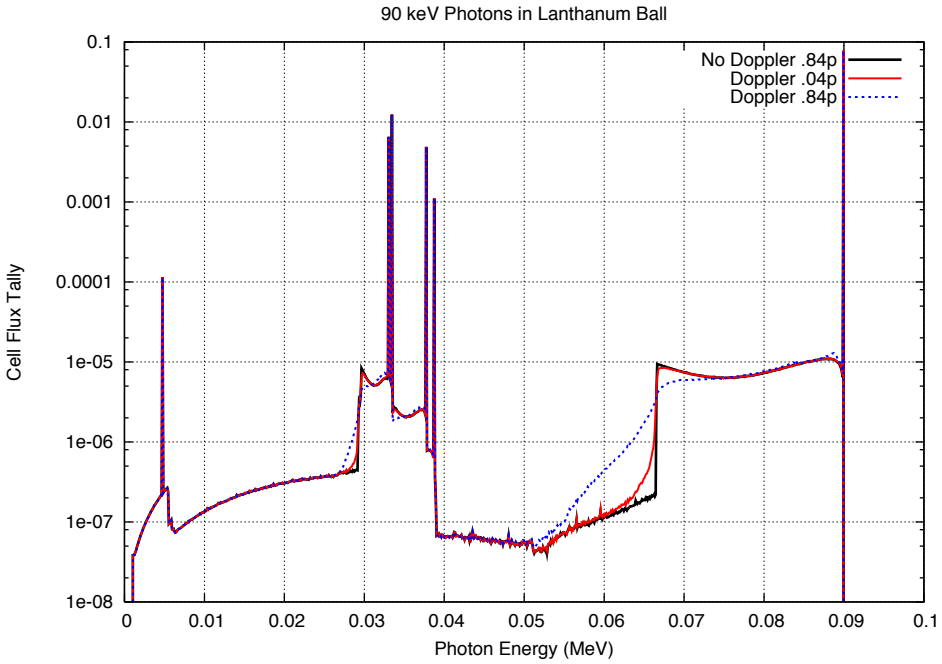

(a)

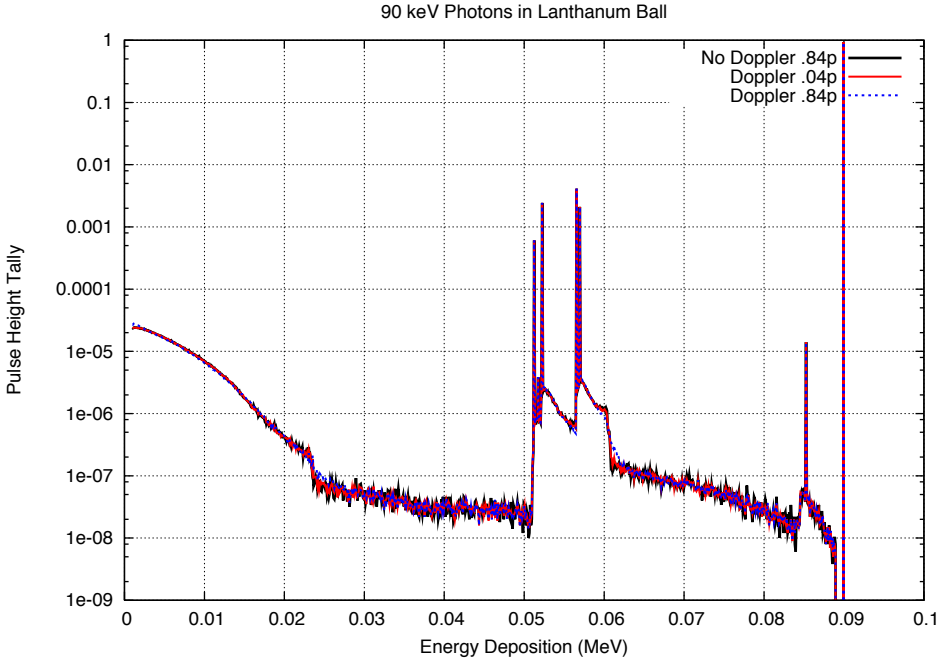

(b)

Figure 30: Cell flux (a) and energy deposition (b) tallies in a Lanthanum ball.

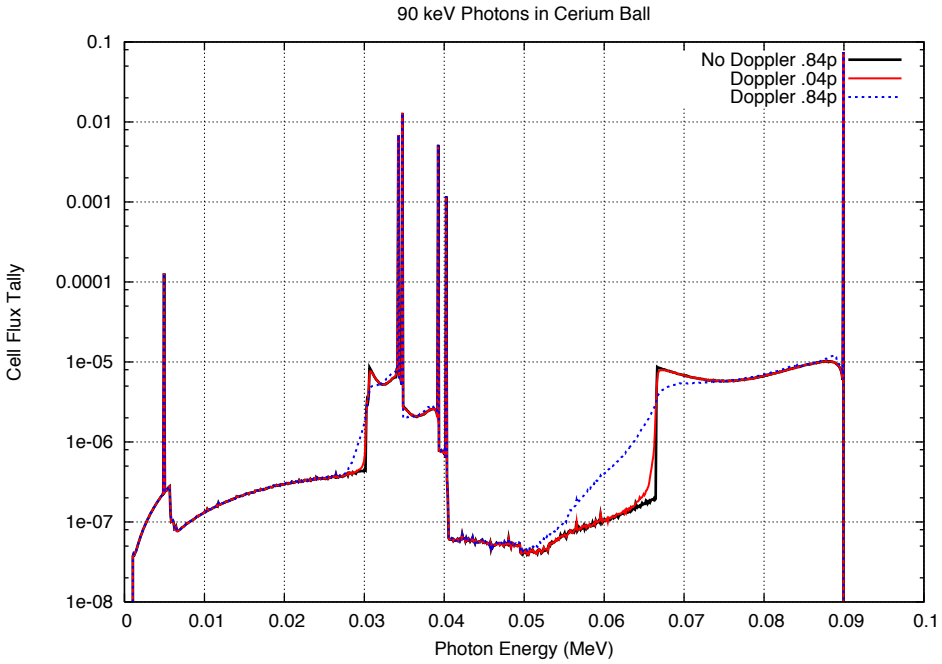

(a)

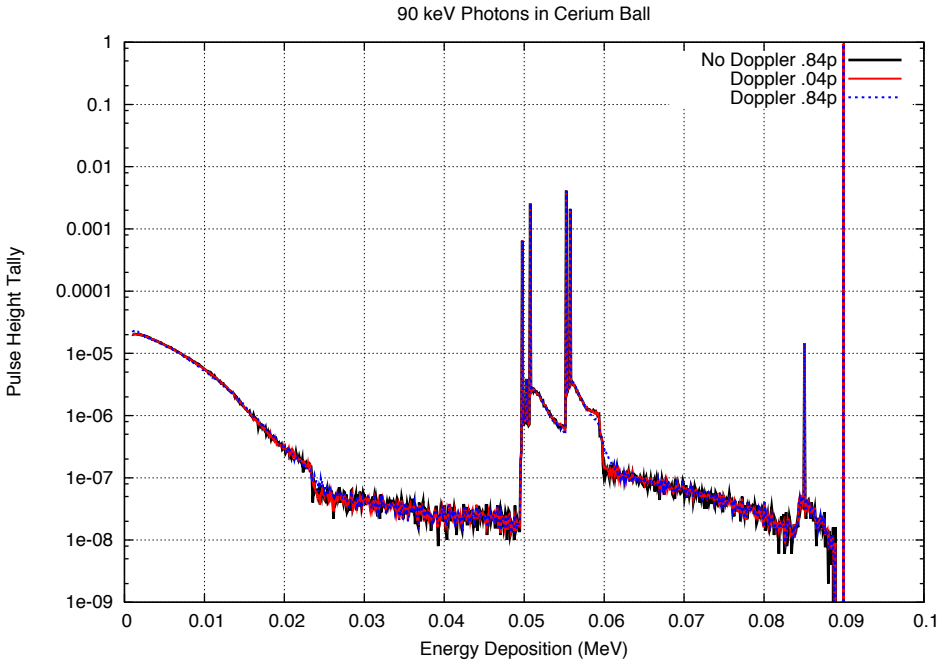

(b)

Figure 31: Cell flux (a) and energy deposition (b) tallies in a Cerium ball.

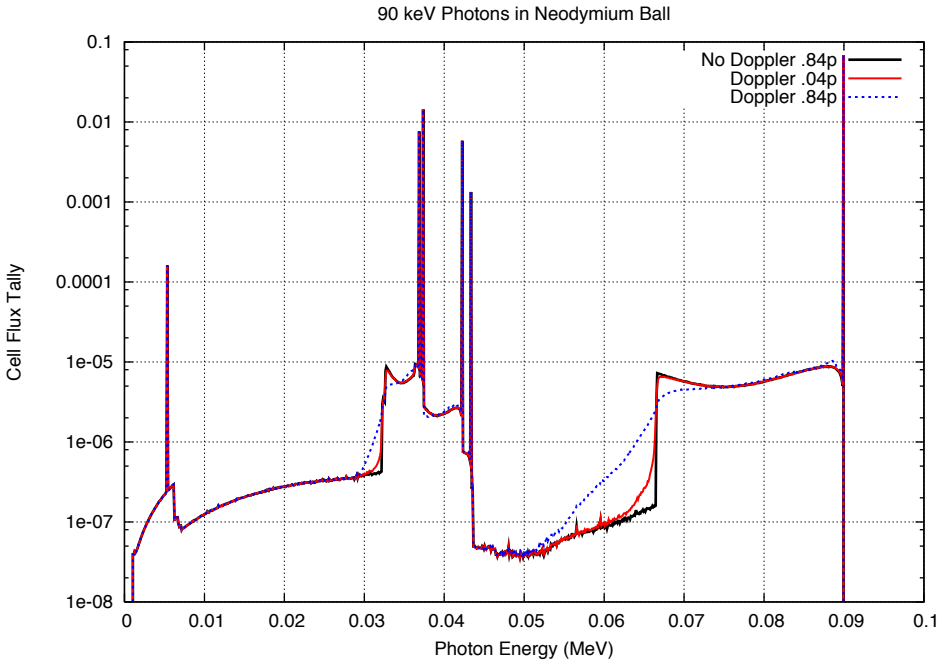

(a)

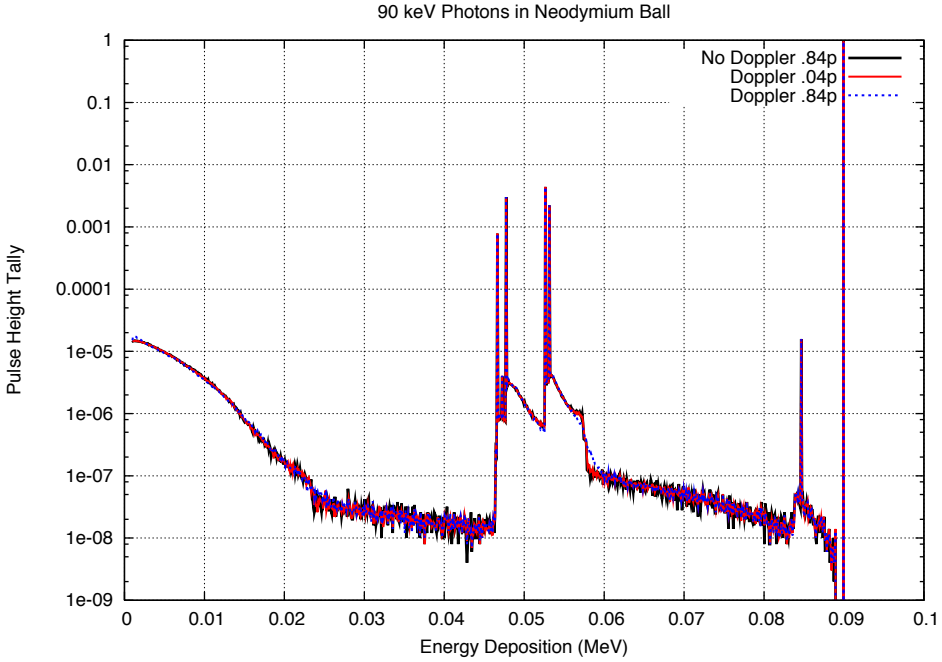

(b)

Figure 32: Cell flux (a) and energy deposition (b) tallies in a Neodymium ball.

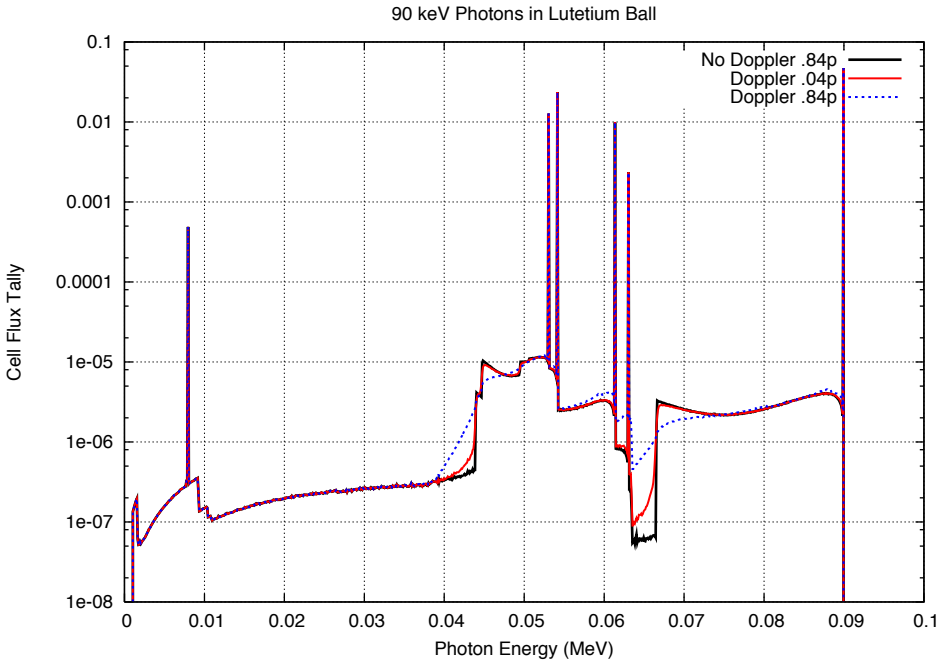

(a)

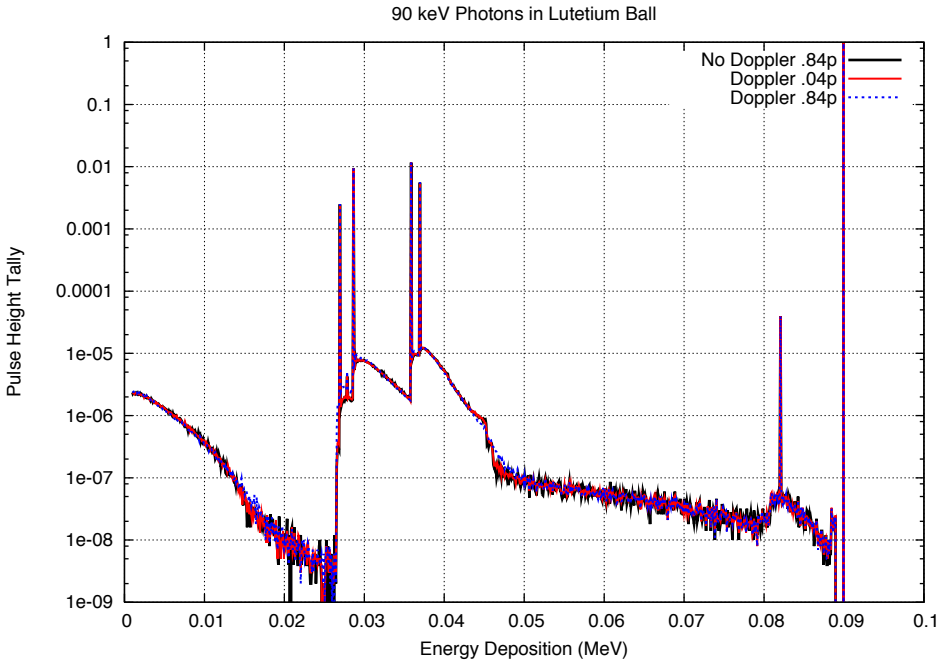

(b)

Figure 33: Cell flux (a) and energy deposition (b) tallies in a Lutetium ball.

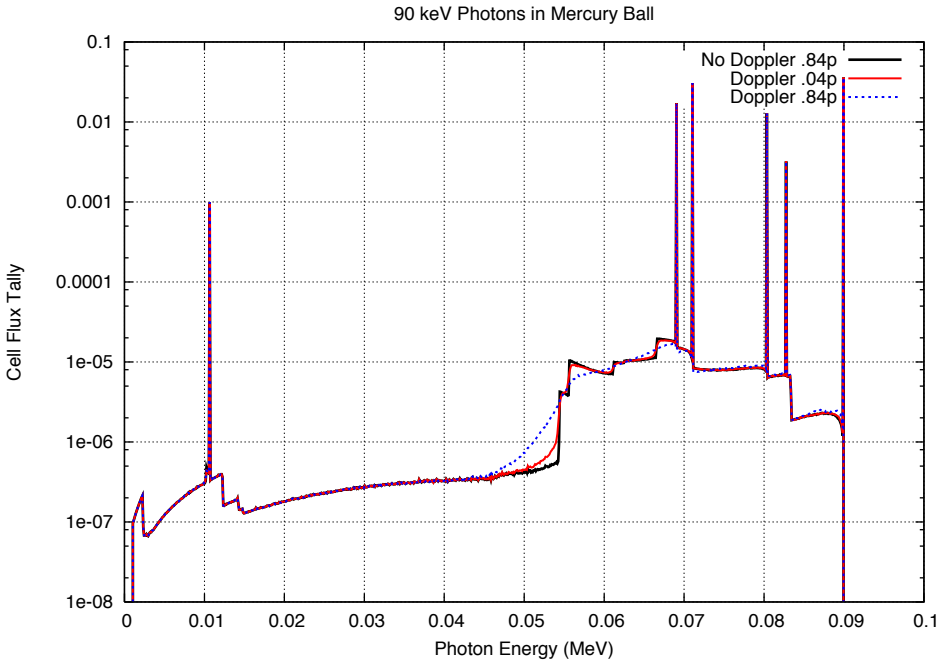

(a)

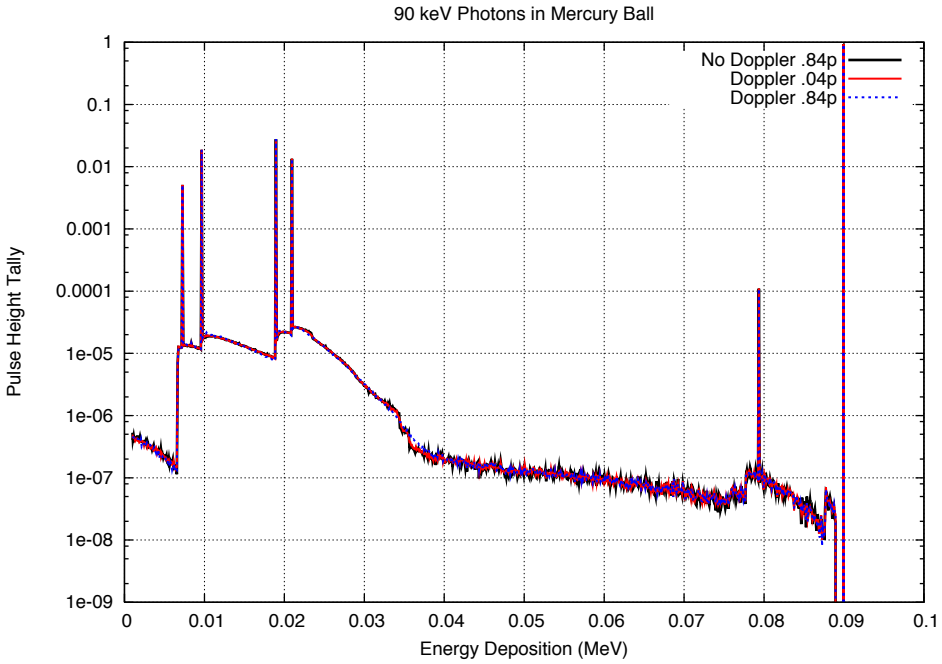

(b)

Figure 34: Cell flux (a) and energy deposition (b) tallies in a Mercury ball.

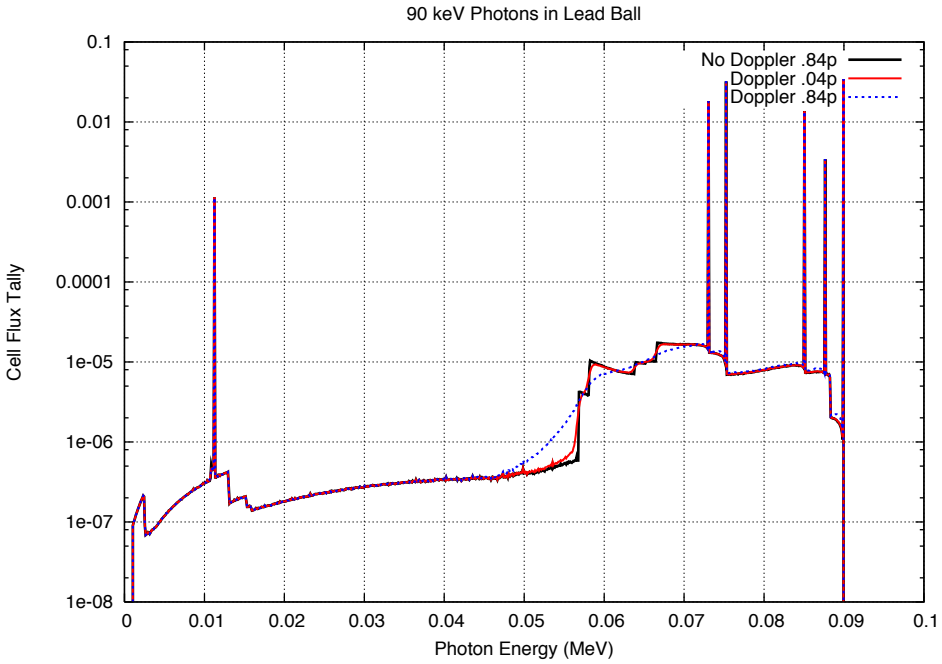

(a)

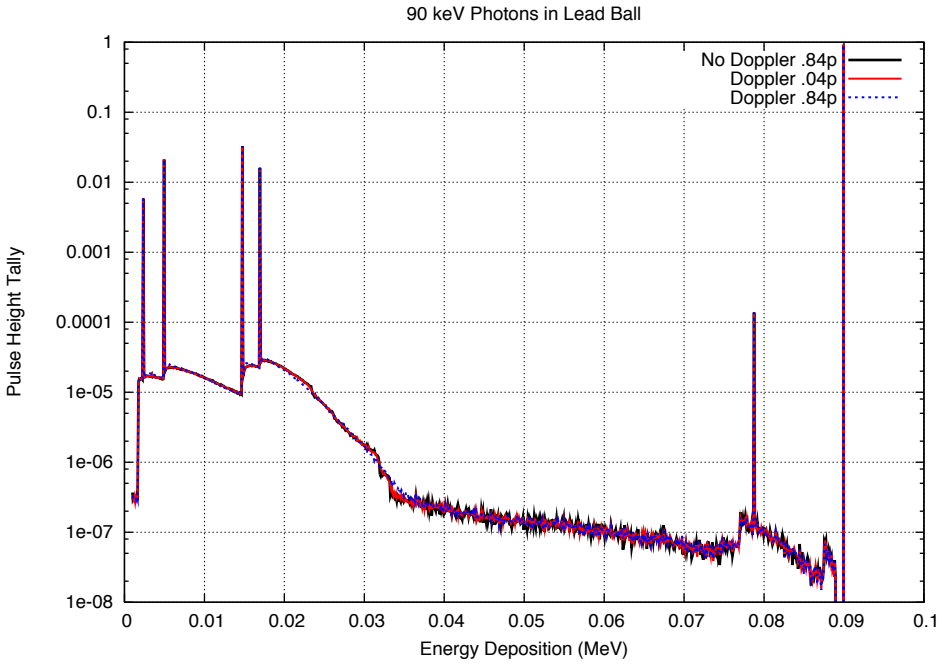

(b)

Figure 35: Cell flux (a) and energy deposition (b) tallies in a Lead ball.

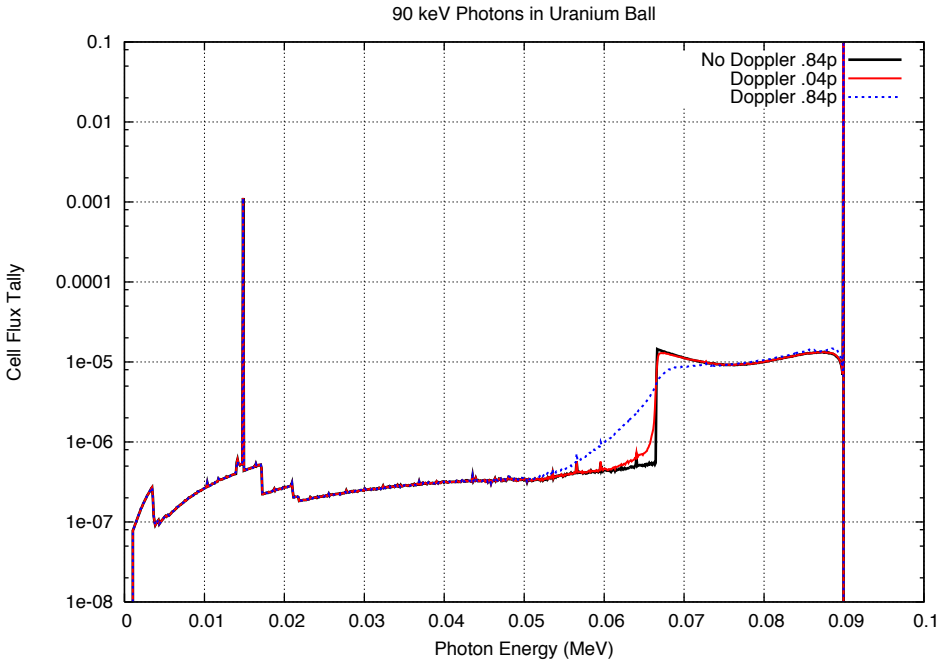

(a)

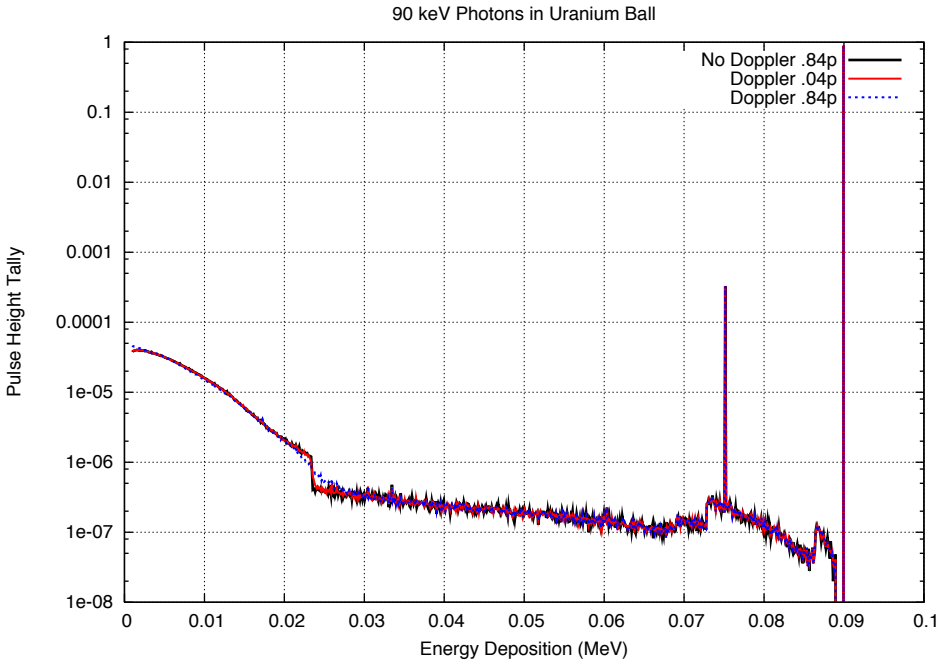

(b)

Figure 36: Cell flux (a) and energy deposition (b) tallies in a Uranium ball.

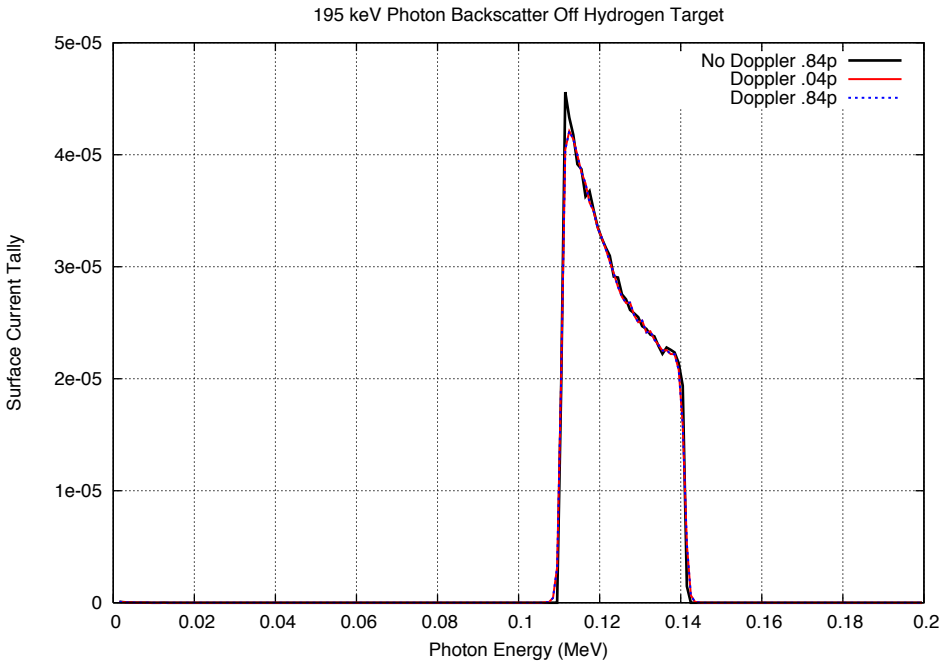

Figure 37: Photon backscattering off Hydrogen target.

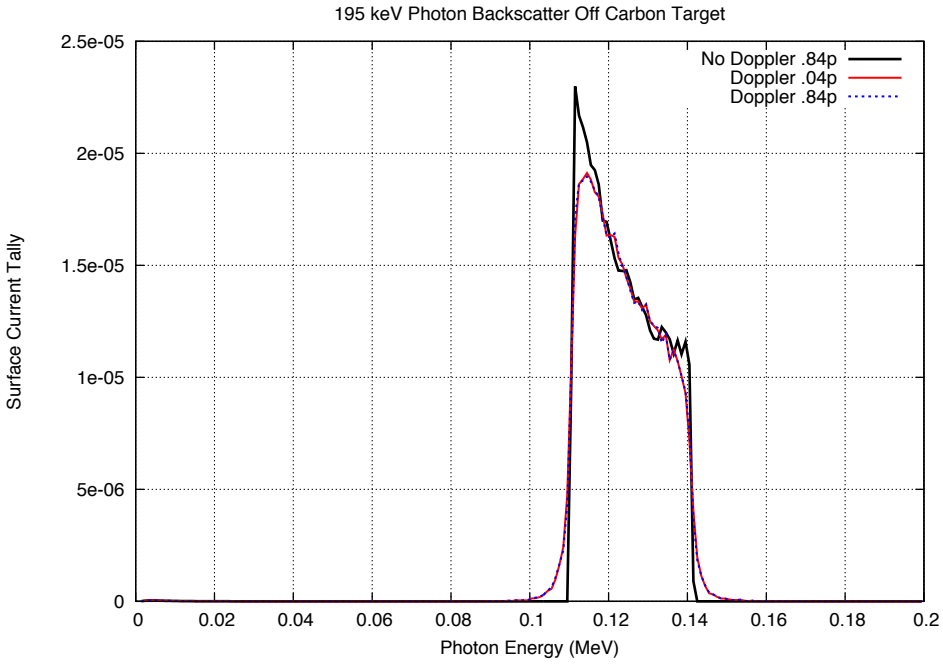

Figure 38: Photon backscattering off Carbon target.

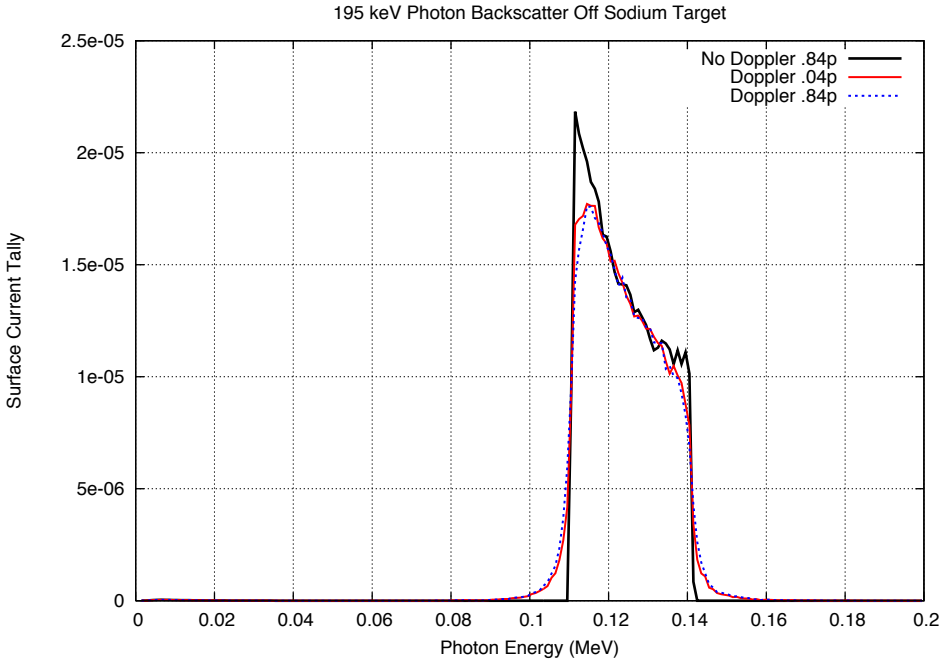

Figure 39: Photon backscattering off Sodium target.

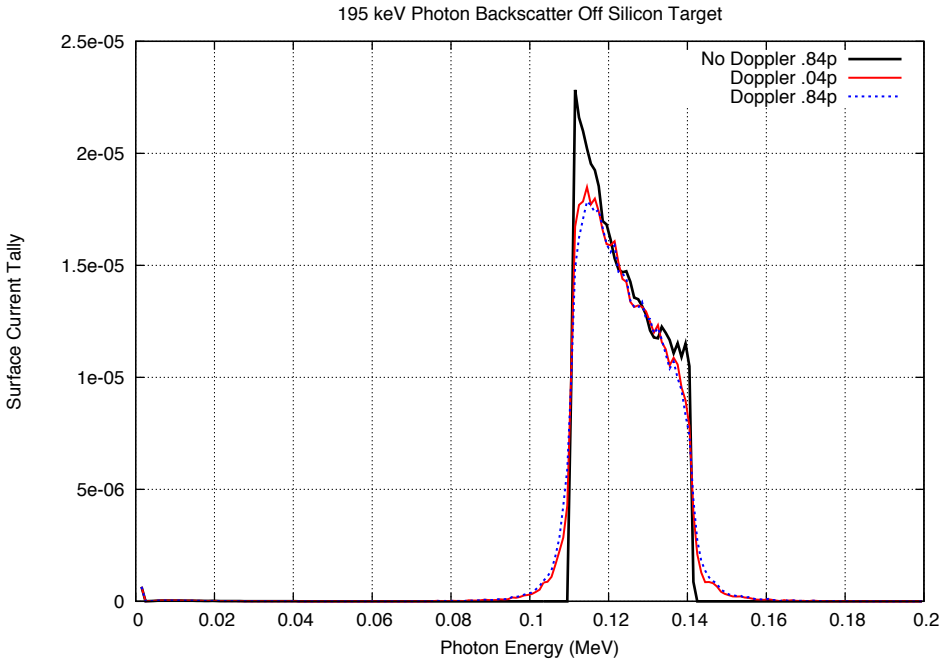

Figure 40: Photon backscattering off Silicon target.

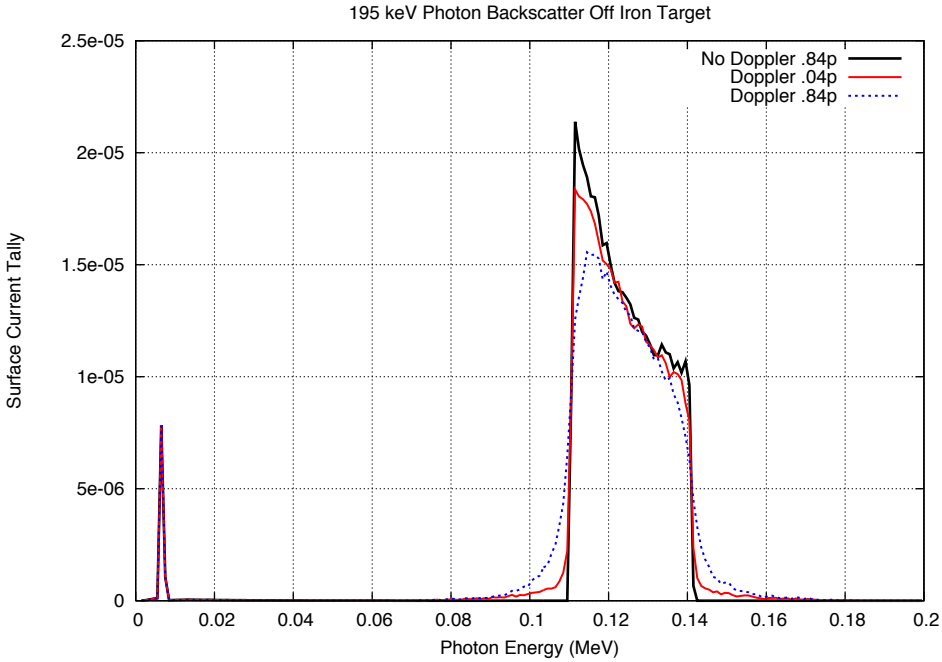

Figure 41: Photon backscattering off Iron target.

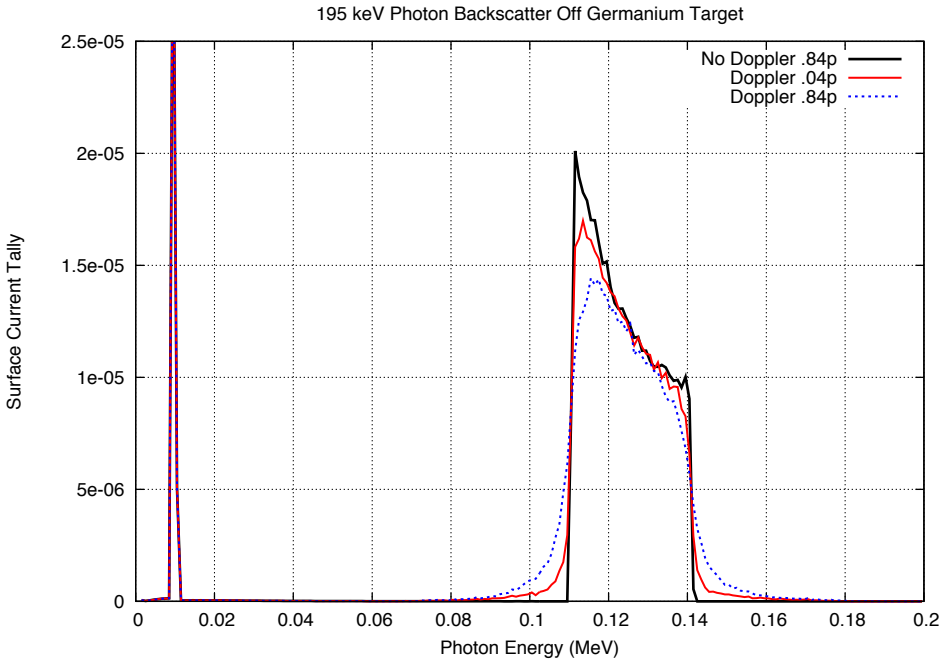

Figure 42: Photon backscattering off Germanium target.

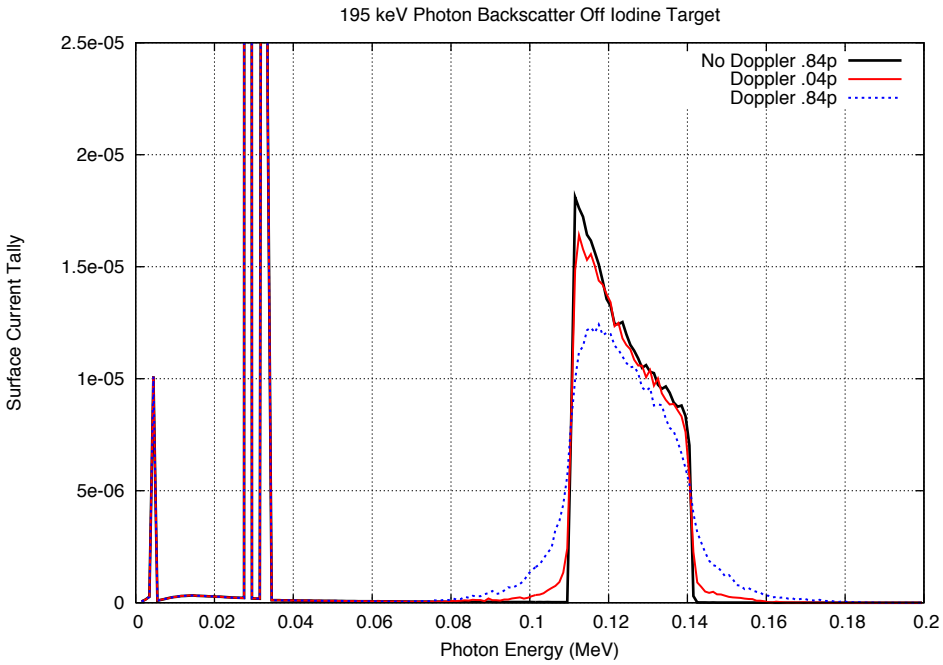

Figure 43: Photon backscattering off Iodine target.

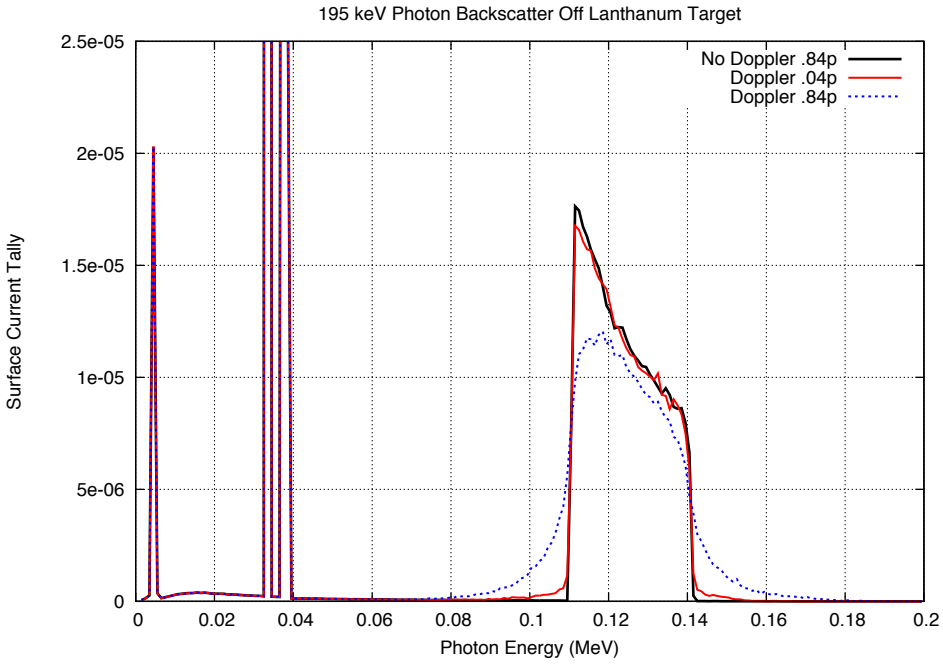

Figure 44: Photon backscattering off Lanthanum target.

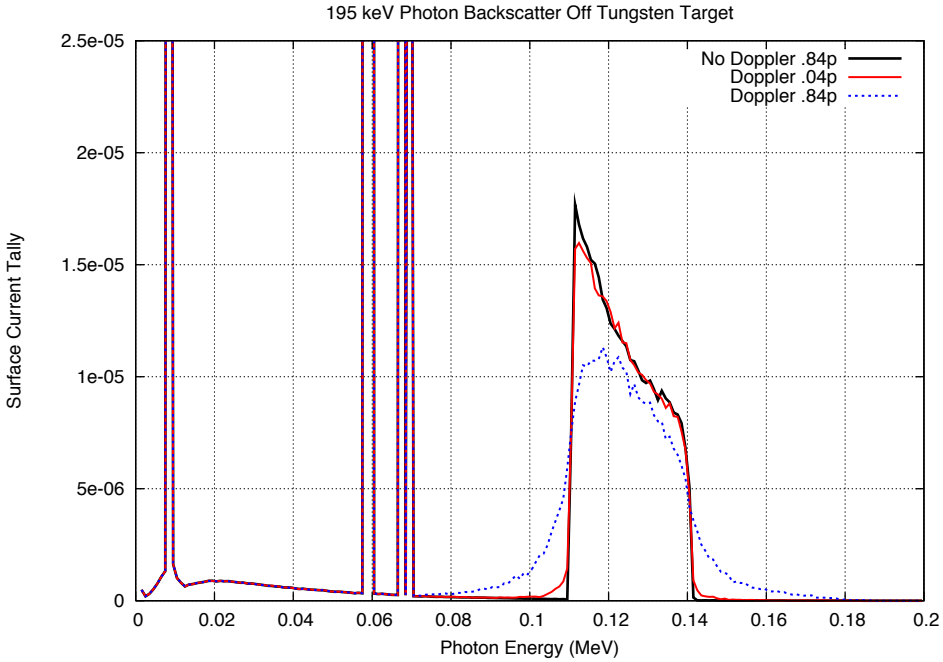

Figure 45: Photon backscattering off Tungsten target.

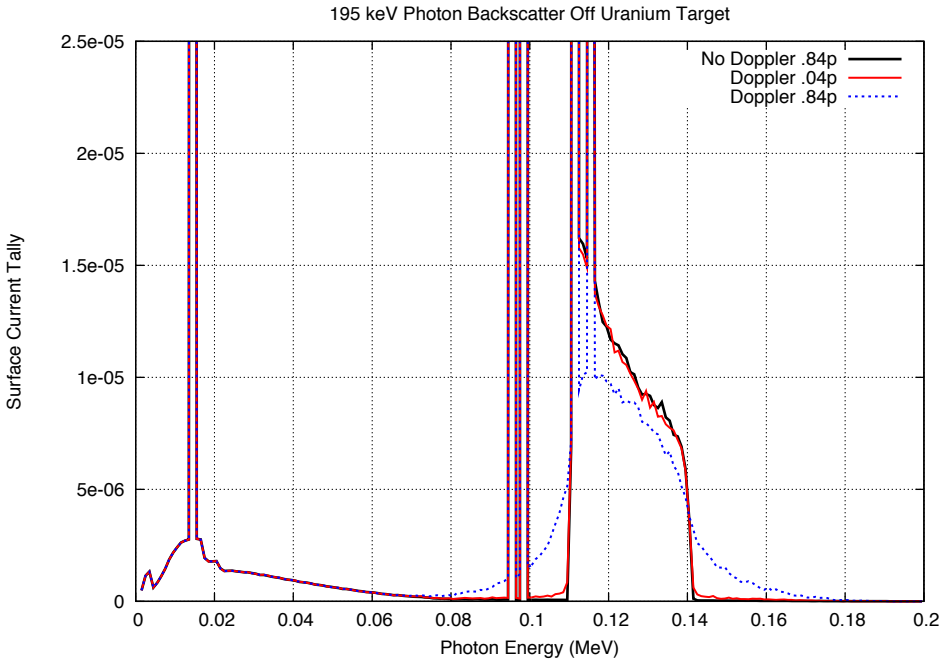

Figure 46: Photon backscattering off Uranium target.

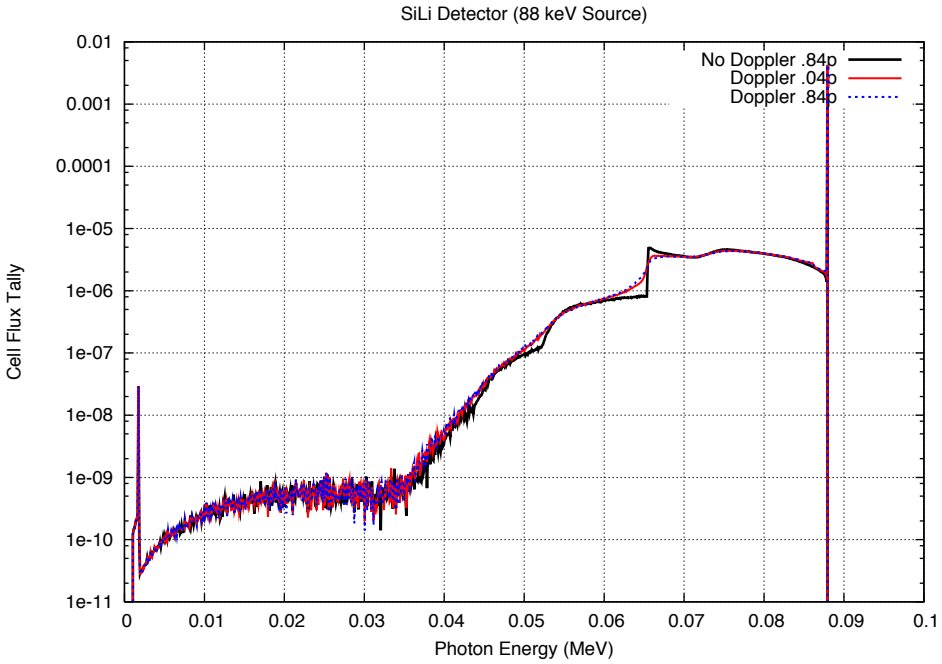

(a)

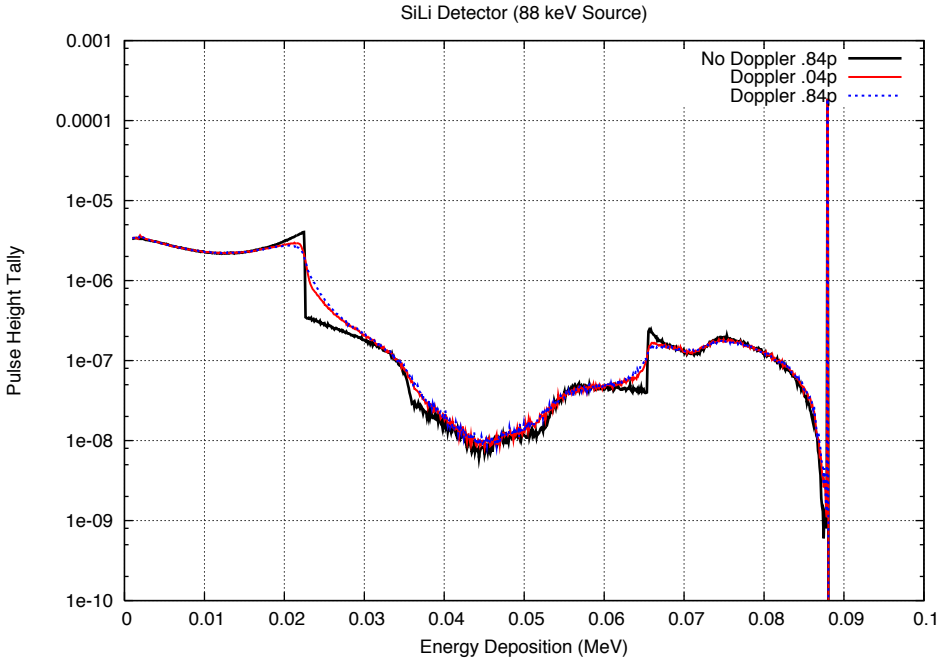

(b)

Figure 47: (a) Photon cell flux and (b) energy deposition inside SiLi detector.

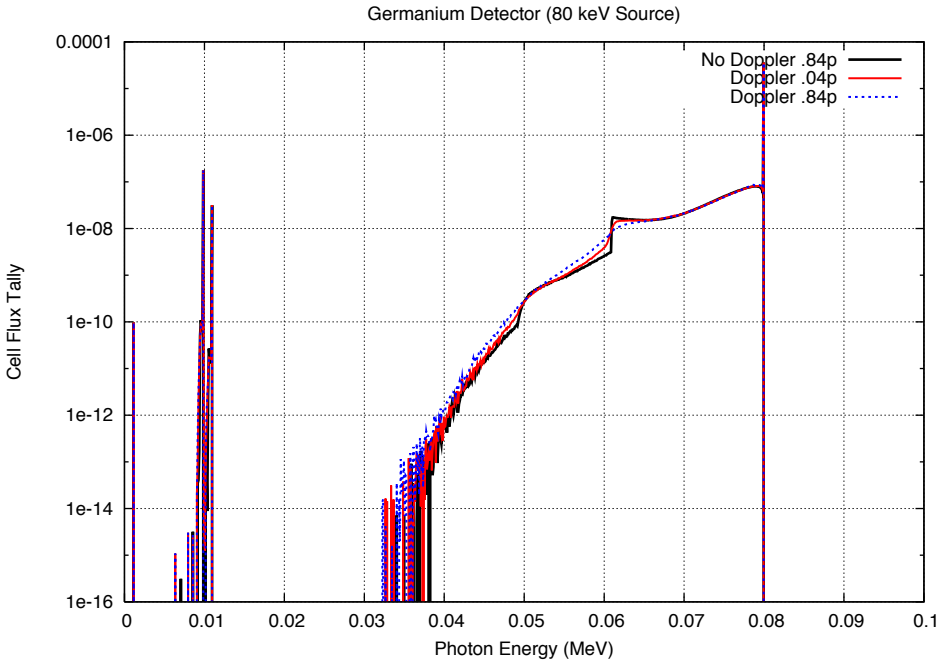

(a)

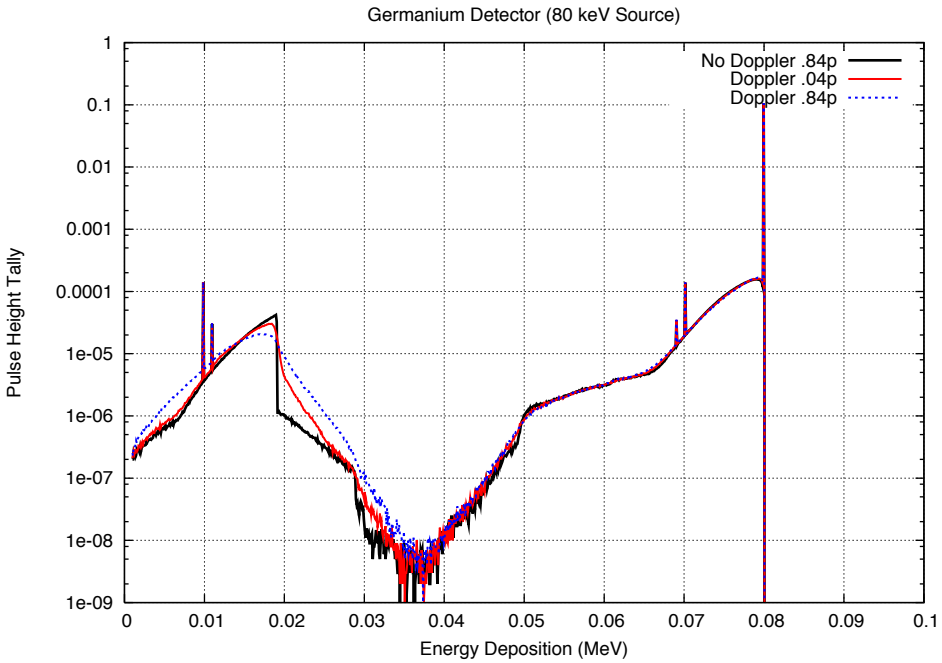

(b)

Figure 48: (a) Photon cell flux and (b) energy deposition inside Ge detector.